DISTRIBUTED ACOUSTIC SENSING FOR DETECTION OF DEFECTS IN THE TEST DAM AT ÄLVKARLEBY – PHASE 2

REPORT 2022:874

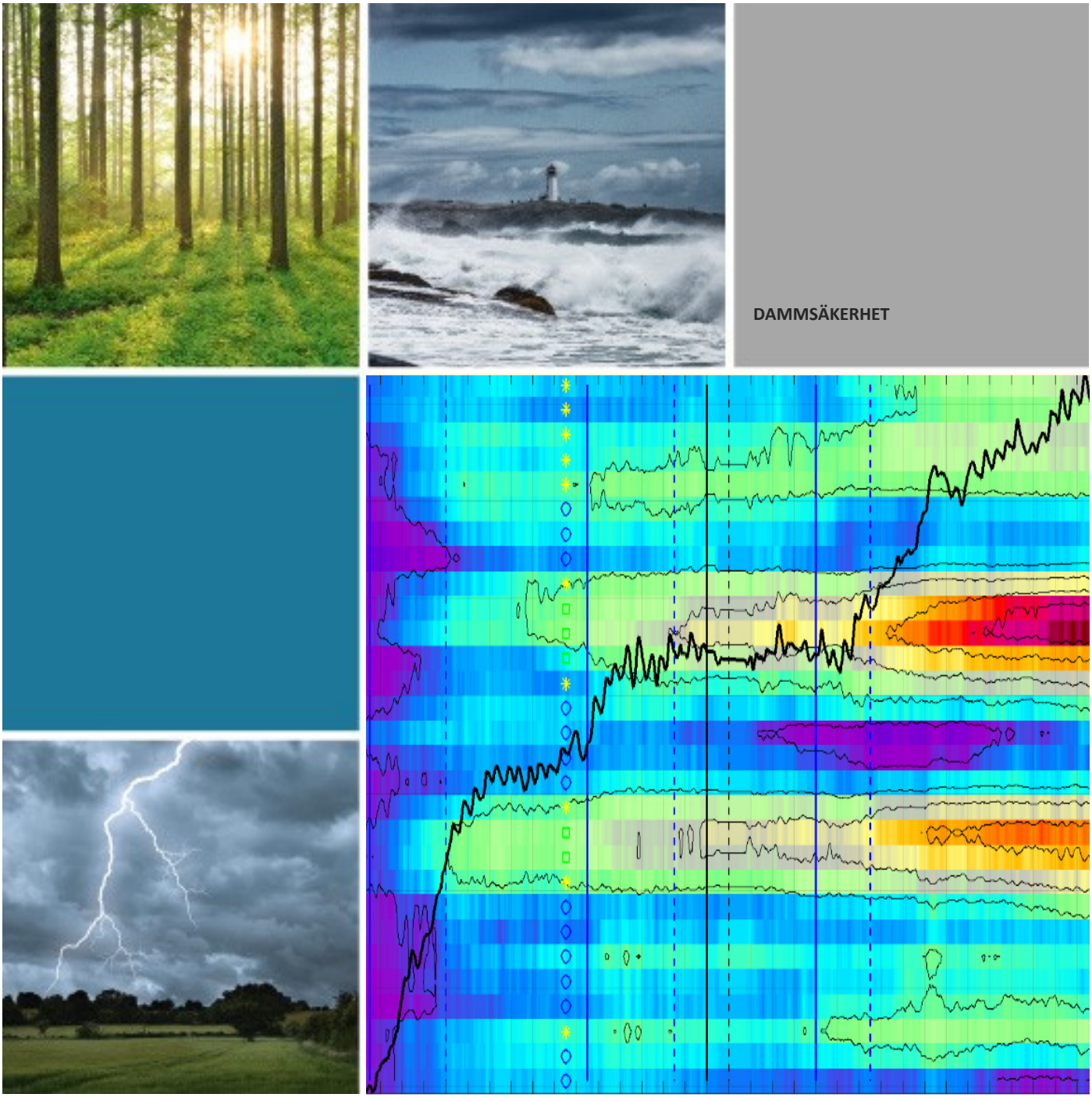

Energiforsk

Distributed Acoustic Sensing for Detection of Defects in the Test Dam at Älvkarleby – Phase 2

SAM JOHANSSON
SOPHIE BEAUPRETRE
AURELIEN MORDET
ANNA STORK

ISBN 978-91-7673-874-0 | © Energiforsk July 2022

Energiforsk AB | Phone: 08-677 25 30 | E-mail: kontakt@energiforsk.se | www.energiforsk.se

Foreword

This project builds on the project *Distributed Acoustic Sensing for Detection of Defects in the Test Dam at Älvkarleby* (Energiforsk report 2021:732). The report describes the passive DAS measurements made during decreasing water levels and carried out over three months. Data evaluation has been performed using Ambient Noise Interferometry using both direct waves (for imaging) and coda waves (for monitoring).

The work has been performed by HydroResearch (Sam Johansson, project leader), Silixa Ltd (Anna Stork) and Sisprobe S.A.S (Sophie Beaupretre and Aurélien Mordret). The work has been followed by a reference group consisting of Henrik Arver, Swedish Regulation Enterprises, Erik Nordström, Vattenfall, Kerim Genel-Waldenström, Vattenfall, Sezar Moustafa, Fortum, and Petter Westerberg, Uniper.

The project has been carried out in the framework of the Energiforsk Dam Safety R&D Program with participation from the Swedish hydropower industry and Svenska kraftnät. The authors are responsible for the content.

Utökad sammanfattning

Optiska fibrer finns numera installerade i flertalet fyllningsdammar i Sverige och är numera så gott som standard vid ombyggnad och nybyggnad. Den vanligaste tillämpningen är övervakning av läckageflöden baserat på temperaturmätningar, men även töjningsmätningar för detektion av rörelser utförs. Många installationer kan även användas för distribuerad akustisk mätning (Distributed Acoustic Sensing, DAS). Under de senaste åren har denna teknik utvecklats markant såväl beträffande mätteknik som utvärderingsmetodik. Akustiska mätningar medför därmed ytterligare möjligheter att studera fenomen som rör läckage/inre erosion i fyllningsdammar.

Akustiska mätningar gjordes i den 20 m långa experimentbyggnadsdamm som byggts av Vattenfall i Älvkarleby. I dammen har fiberoptiska kablar installerats för mätning av temperatur, töjning och akustiska signaler. Dammen har sex inbyggda defekter som alla representerar skador som så småningom skulle kunna leda till ett dammhaveri. Var dessa defekter finns är inte känt för rapportförfattarna.

Undersökningarna/övervakningen inleddes våren 2020 (kallad Fas 1). Resultatet från DAS-mätningar under den första inledande fyllningen (dvs. vid transienta förhållanden) visade lovande resultat, men identifierade även områden där ytterligare förbättringar kunde göras (Johansson et al. 2021). Några av dessa har tillämpats i den här studien för de mätningar som utfördes under hösten 2021 (Fas 2).

Denna rapport beskriver resultatet av de akustiska mätningar som utförts efter att dammen varit i drift vid högt vattenstånd i över ett år. Det är då rimligt att anta att stationära förhållanden avseende vattenmättnad råder. Mätningarna utfördes under nästan tre månader (från mitten av augusti till början av november 2021). Genom att avsänkning av vattennivån gjordes i olika steg kunde förändringen av skjuvvågshastigheterna i dammen följas.

Skjuvvågshastigheten beror främst av materialets densitet och skjuvmodul, men även temperatur och tryck har viss inverkan. Med inledande resonemang och modellering erhölls viss information om vilka hastighetsförändringar som uppkommer vid de olika material som förekommer i de inbyggda defekterna, samt vid förändring av magasinsnivån.

Datautvärderingen har utförts med hjälp av interferometri, baserad på analys av omgivande brus (Ambient Noise Interferometry, ANI) där två olika metoder använts. Den första metoden kallas ”Imaging” där direkta vågor analyseras för bestämning av skjuvvågshastigheten i dammen vid en given tidpunkt. I den andra metoden kallad ”Monitoring” analyseras coda-vågorna för mätning av den relativa hastighetsförändringen i detta fall var 30:e minut under hela mätperioden (Fas 2). Tack vare den distribuerade mätning fås information med hög upplösning längs dammen. Förnyad utvärdering med den senare metoden har även gjorts om för Fas 1, med användande av de förbättrade rutiner som tagits fram sedan föregående utvärdering.

Endast mätresultat från fibern på tätkärnans krön redovisas eftersom en första analys av korrelationerna mellan fibrerna uppströms och nedströms tätkärnan

visade att dessa mätningar dessvärre inte har tillräcklig noggrannhet vid mätning i denna skala. Vid redovisningen har därför alla djup beräknas från nivån på krönkabeln.

Vid analys av mätningarna med ”Monitoring” framkommer att det är möjligt att upptäcka små hastighetsförändringar med hög noggrannhet och med god rumslig upplösning längs dammen. Viss information om på vilket djup störst förändringar sker erhålls även i detta fall eftersom mätning gjorts vid olika vattenstånd. ”Imaging” är mindre exakt beträffande detektion av hastighetsförändringar, men har fördelen av den även ger informationen om på vilket djup som förändringar sker.

Kombinationen av de båda metoderna ger därför bättre förutsättningar att bestämma var hastighetsförändringar sker. Generellt gäller att ”Monitoring” samlar information inom en större volym (tack vare coda-vågornas egenskaper) än den information som ”Imaging” ger, vilken baseras på den information som de direkta vågorna ger.

Simuleringar av defekternas påverkan av skjuvvågshastigheten utfördes för att ge vägledning vid tolkning av hastighetsförändringarna. Såväl förändring orsakad av ändrade materialegenskaper som varierande vattenstånd beaktades.

En förbättrad analys av data från Fas 1 gjordes, vilken visar att vi bättre kan lösa upp de hastighetsförändringar som är kopplade till de olika vattennivåerna i magasinet. Resultat från Fas 2 är annars mest tillförlitligt på grund av förbättrad mätnoggrannhet jämfört med Fas 1. Dessutom har de transienta effekterna beträffande vattenmättnad avtagit, och dessa effekter är därför mindre än i Fas 1. Anomalier som identifieras av både ”Imaging” och ”Monitoring” i Fas 2 ger därför den starkaste indikationen på att hastighetsförändringar uppkommit.

De mest sannolika platserna för defekter finns runt sektionerna 11, 13, 17 och 19 m, där en god överensstämmelse framträder mellan ”Imaging” och ”Monitoring” både i Fas 1 och Fas 2. Vid sektion 5 m framkommer också en god överens-stämmelse mellan båda metoderna i Fas 2. Anomalierna vid sektion 17 och 19 m kan bestå av betong- och träkuber, men tecken finns även på vissa förändringar skett i tätkärnematerialet eller att vattenströmning förekommer.

Tecken på horisontella defekter genom tätkärnan kan ses i sektion 5 och 11 m i dammens djupare del. Den vertikala cylindern med grovt material kan vara den anomali som ses vid sektion 13 m.

Resultaten och erfarenheterna från detta projekt är lovande och mätningar på typiska dammar kan utföras med de metoder som utvecklats och använts här, både för undersökning (kortvariga mätningar) och för kontinuerlig övervakning. För bäst resultat rekommenderas att metoderna kombineras samt att mätning görs under längre tid, gärna vid olika vattenstånd.

Ytterligare forskning rekommenderas för att fortsätta metodutvecklingen, särskilt för att bättre förstå orsaken till de seismiska hastighetsförändringarna i dammen.

Nyckelord: Distribuerad akustisk mätning, Inteferometrisk analys av omgivnings-ljud, detektion av skador och inre erosion i fyllningsdammar, blindtest.

Summary

Optical fibres for dam monitoring are widely used in existing embankment dams and their installation is almost a standard in new dams in Sweden today. The most common application is seepage flow monitoring based on temperature measurements, but strain measurements are also used. Recent developments in Distributed Acoustic Sensing (DAS) technology and DAS data processing techniques for monitoring and analysis offer another way to study seepage/ internal erosion phenomena in dams. The application of this monitoring technology will be easy to apply especially in dams where fibres are already installed.

Vattenfall has designed and built an experimental embankment dam with six built-in defects that all represent damages that eventually could evolve to a dam break. The locations of these defects are still not revealed. Fibre optic cables are installed in the experimental dam for measurement of temperature and acoustic signals.

Result from DAS measurements during the first initial filling in 2020 (Phase 1) showed promising result, despite the transient conditions in the dam. This report describes the passive DAS measurements made during decreasing water levels and carried out over three months in 2021 (Phase 2). Data evaluation has been performed using Ambient Noise Interferometry using both direct waves (for imaging) and coda waves (for monitoring) during the entire recording period. In addition, a further evaluation of the monitoring data from Phase 1 has been carried out.

An improved analysis of Phase 1 data shows we are able to resolve the seismic velocity changes associated with each step change in water-level. The results from Phase 2 are the most reliable due to improved monitoring accuracy compared to Phase 1 and less transient effects with lowering of the water level. Anomalies identified by both the imaging and monitoring analyses in Phase 2 thus provide the strongest indication of a defect.

The most probable locations defects are around Sections 11, 13, 17, and 19 m, where we see a good agreement between the imaging and monitoring results in Phase 2 and also imaging/monitoring results from Phase 1. At Sec 5 m we see agreement between both methods in Phase 2. The anomalies at Sec 17 and 19 m might be the concrete and wooden cube but with some changes to the core material/water leakage around the edges of the defects. The horizontal damage crossing the core might be seen in Sec 5 or 11 m in the lower part of the dam. The vertical cylinder with coarse material may be the anomaly seen at Sec 13 m.

The results and the experience gained in this project are promising and measurements on large dams can be performed using the methods developed, both for investigation purpose (short-time measurements) and for continuous monitoring. Further research is recommended to continue the method development, especially for better understanding of the cause of seismic velocity changes in the dam.

Keywords: Distributed Acoustic Sensing, Ambient Noise Interferometry, embankment dams, detection of defects, internal erosion, blind test.

List of content

1 Introduction

The use of optical fibres for dam monitoring started in 1998 in Sweden. The technology is widely used in existing embankment dams and is almost a standard in new dams in Sweden today. The most common application is seepage flow monitoring based on temperature measurement, but also strain measurements are used. With these two methods it is possible to measure, with high accuracy and high spatial resolution, the two most fundamental parameters in dam surveillance: seepage and movements. By adding acoustic measurements, information will also be obtained regarding material property changes in the dam body at greater distances from the optical fibre.

Recent developments in Distributed Acoustic Sensing, DAS, technology and DAS data processing techniques for monitoring and analysis, may give an additional method to study seepage/internal erosion phenomena in the dams. The application of this monitoring technology will be easy to apply especially in dams where fibres are already installed. A first test was made in 2019 (Johansson et al., 2020).

Vattenfall has, in accordance with the Swedish dam safety guideline (Swedenergy 2017), designed and built an experimental embankment dam at their laboratory facilities in Älvkarleby. The dam has six built-in defects, that all represent damages that eventually could evolve to a dam break. These defects are sized to be realistic, while still large enough to be realistically detected in blind-tests by suitable geophysical methods.

The investigations/monitoring began in Spring 2020. The location and size of the defects is not yet revealed. Several methods will be applied by different institutions and companies both for short-term measurements (in terms of campaigns) and long-term measurement. Fibre optic cables are installed for measurement of temperature, strain, and acoustic signals. Result from DAS-measurements during the first initial filling (i.e., at transient conditions) showed promising result, but also areas for further improvement (Johansson et al. 2021). Some of those have been applied in this study. Further evaluation of the data has also been performed with funds from EIT Raw Materials Booster program (grant n° 15099-CCLC-2020-6; Mordret, et al., 2022).

This report describes the acoustic measurements carried out after the dam have been in operation at high water level for over a year. Measurements were performed for almost three months (mid August – early November 2021). Initial stationary conditions regarding saturation are reasonable to assume, and the transient conditions at lowering the water level will give information of the change in material properties.

The work on site was performed by Carl Nygren and Sam Johansson, HydroResearch. Measurements were set-up remotely by Anna Stork and Ariana David at Silixa, who also assured the data quality. The final seismic data analyses were made by Aurélien Mordret and Sophie Beauprêtre, Sisprobe, using the Ambient Noise Interferometry (ANI) approach (Curtis, et al. 2006).

2 Objective

Existing methods can detect seepage changes close to the measurement point, or along a line (with distributed sensing). Sometimes this is good enough, but there is also sometimes a need to obtain information over a larger volume. This can be achieved using DAS because it has the ability to detect changes in the propagation of the seismic waves, caused by material changes far away from the fibre optic cable and identify events that can create seepage flow changes. Both passive and active measurement techniques could be used.

Based on the promising result from the previous test in 2020 (Phase 1) we concluded that further development was possible, and these objectives/actions were identified:

- Monitoring of seismic velocity variations at different water levels using an improved DAS-interrogator
- Use intra- and inter-fibre correlations to measure changes in velocity. The proposal is to use two fibre lines for inter-fibre correlations.
- Poroelastic modelling to quantify observed seismic velocity changes.
- Eikonal tomography to image dam at three water levels during the monitoring period
- Time lapse eikonal tomography performed at regularly spaced time intervals. This would improve understanding of the state of the dam between the full and empty stages of the filling cycle.
- Tests for 3D imaging and monitoring. This would include testing imaging and monitoring between different pairs of cables.

3 Application of DAS in the experimental dam

3.1 BACKGROUND

The design of the test dam was based on experiences of a previous blind test in Norway in 2003 where the potential of resistivity, self-potential and temperature surveying was undertaken on a rockfill embankment dam (Johansson, 2005). The dam, with a height of 5.25 m and a length of 37 m, was built with a central core of moraine with supporting rock fill and with in-built defects. It was known from a desktop sensitivity study based on the material properties of the building materials that it would not be possible to detect small defects using single campaign surveys. However, geophysicists managed to indicate defect locations by testing a monitoring approach investigating changes over time.

The Norwegian blind-test dam was not built as a conventional earth embankment dam, where there would normally be filters separating the impermeable core from the outer coarse pervious shell (rock fill). The experimental dam at Älvkarleby, was however designed in accordance with the Swedish dam safety guidelines.

3.2 THE ÄLVKARLEBY TEST DAM

The chosen embankment dam design is a 20-meter-long dam where the impermeable core is supported by two connecting filter zones and support fills (Figure 1). The height is 4 meters, and its base against the foundation perpendicular to the dam line is 15 meters. The two sidewalls which the dam connects to are slightly angular (12,5 %). The bottom slab is inclined 1% towards the downstream side, where a ditch collects the seepage water through the dam body. This seepage is divided by ribs into eight sections which are continuously monitored by flow. However, the result will be revealed in the end of the experimental dam project.

The dam rests on a rigid concrete support structure submerged into a riverbank of 12 meters of sand overlying bedrock (drained conditions). The experimental dam thus has its crest in line with the surrounding ground. To the extent possible, the design is made to avoid structural members with negative impact on geophysical measurements. The bottom concrete slab of the containment has therefore been reinforced with fibreglass reinforcement bars. Since there is no electrically conductive reinforcement this resembles foundation on rock.

From an acoustic point of view the surrounding concreate walls will create seismic wave reflections which will complicate the evaluation. The acoustic environment at the test dam will thus be more complicated than when measuring in real embankment dams.

Figure 1 Pictures of the crest and downstream face and upstream face of the test dam before filling.

The built-in defects, that all represents damages that eventually could evolve to a dam break, are:

1. Cavity in the core (wood cube 0.4 m × 0.4 m × 0.4 m).
2. Horizontal permeable zone passing through the core (rectangular cross section 0.1 m high and 0.5 m wide).
3. Vertically loose zone (elongated zone with square cross section with side 0.3 m).
4. Lump of concrete or large stone (cube 0.5 m × 0.5 m × 0.5 m).
5. Permeable horizontal zone at side (0.1 m x 0.1 m).
6. Filter defect on the upstream side.

Being a blind-test, the position of these defects is not known to the investigators (in fact kept secret to a few persons only). They will be revealed later.

3.3 CABLE INSTALLATIONS

The cable installation (as showed in Figure 2) is extensive compared to typical installation in large dams, where normally just one or a few cables are installed along the dam. In the test dam there is one cable, placed at four levels in the upstream filter, and on the core crest. Some parts of this cable are also placed in water, allowing the water temperature to be measured. A second cable was used to measure at five levels in the downstream filter, and a third cable is placed closed to the dam toe.

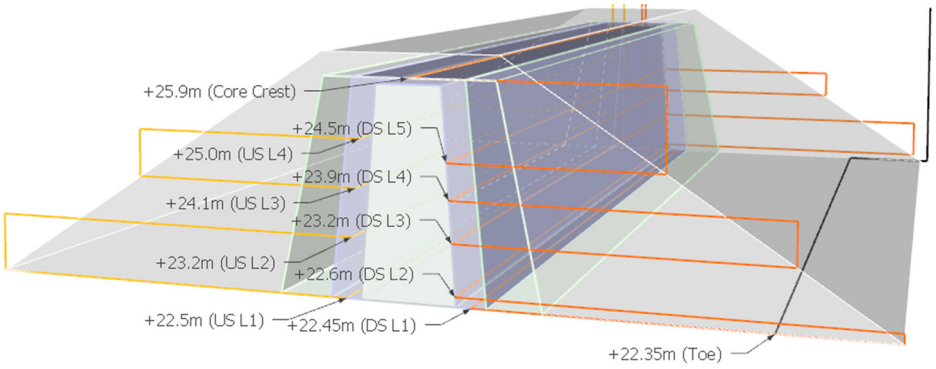

Figure 2 Cross section of the dam showing the three installed cables (Yellow, orange and black).

All cables contain both multimode and single mode fibres. This enables DTS, DAS and Distributes Strain Sensing (DSS) measurement. Furthermore, the cable in the downstream toe contains a copper wire, which can be used for heating for the Heat-Pulse test ("Active DTS method").

The dam chainage (CH) along the dam starts on top of the dam at the connection to the sloping concrete wall at the left side (CH 0 m) and ends at the right abutment at CH 20.6 m on the crest. The bottom starts at CH 0.3 m and ends at CH 20.3 m. All data is presented along the dam using dam chainage.

3.4 DISTRIBUTED ACOUSTIC SENSING (DAS) MONITORING TECHNOLOGY

DAS technology has undergone significant development and improvements in the last decade. The technique can be used to effectively measure the speed of sound and seismic waves in soils, rocks and fluids in many different scenarios. Like Distributed Temperature Sensing (DTS), DAS only requires an interrogator unit, a power source and a fibre optic cable to measure dynamic strain (Parker et al., 2014). DAS technology has been deployed for borehole monitoring, ground movement detection, and pipeline monitoring in many industries, such as oil and gas, geothermal exploration, and CO_2 sequestration, and in remote and harsh environments (e.g., Becker et al., 2019; Jousset et al., 2018; Nikles 2009).

DAS measurements are made on fibre-optic cables which may be the same fibre-optic cables installed for temperature sensing. A DAS system provides a sensor array that is unmatched in spatial resolution and sampling capabilities by traditional seismic instruments, while allowing the application of processing methods developed for use with traditional seismic arrays (Lindsey, et al. 2017).

The propagation of the acoustic energy in the ground can be analysed in to determine the speed of sound and assess the ground composition.

The operating principle for DAS is illustrated in Figure 3. A pulse of light is emitted from the DAS interrogator and travels down an optical fibre. Measurements can be made on fibres up to tens of km long and a single-mode or multimode cable can be used with the system. A small amount of the light is naturally scattered in the fibre and returns to the interrogator unit. An optoelectronics architecture in the sensing unit measures the amplitude and phase of the backscattered light. When an acoustic or seismic wave exerts tiny pressure/strain changes on the fibre this changes the amplitude and phase of the backscattered light. The relative phase and amplitude can be used to determine the strain rate on the fibre.

The sensing system measures changes in strain at a rate of up to several tens of kHz, required to accurately record acoustic fields. The system digitally records the response at evenly spaced measurement points or channels along the fibre. The Silixa intelligent DAS (iDAS™) system (Figure 3) can offer spatial sampling of 1-m with a dynamic range of more than 120 decibels and with no cross-talk between adjacent measurements. The spatial resolution, or gauge length, of the system can be tuned to the individual application. Standard gauge lengths are 3 m and 10 m. Short gauge lengths improve the spatial resolution but results in a lower signal-to-noise ratio (SNR).

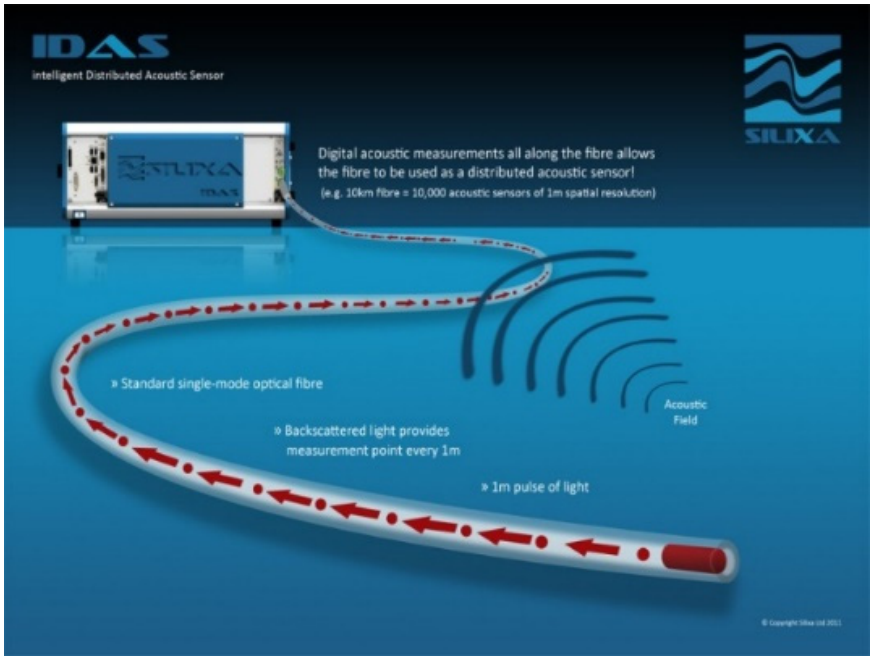

Figure 3 The iDAS™ provides digital acoustic measurements along the entire length of single-mode fibre. The interrogator emits pulses of laser light along the fibre and measures the phase and amplitude of the backscattered light from every measurement point (channel) along the fibre.

The use of DAS for seismic surveys has been validated through the use of traditional seismic processing methods to compare DAS results with those from traditional seismic surveys and laboratory testing (e.g., Jousset et al., 2018; Lindsey et al., 2017; Parker et al., 2014).

3.5 DAS MONITORING SET-UP

An iDAS with a 3 m gauge length was used in this study. This increases noise levels in the data compared to a 10 m gauge length but, given the small horizontal extent of the dam (20 m), the unit with the smaller spatial resolution (3 m) was required. The equipment was installed at site by HydroResearch (Figure 4) and the set-up of the iDAS was performed remotely by Silixa using the parameters given in Table 1. Some example data are shown in (Figure 5). To assess data quality the noise levels were verified to be as expected (Figure 6). The overall noise levels are similar to the data collected during Phase 1 of the project. Calibration "tap tests" to determine channel locations were performed in Phase 1 of the project in 2020 (see Johansson et al., 2020).

Figure 4 Monitoring unit for DAS and DTS, inside the monitoring container.

Table 1 iDAS parameters used in data acquisition.

Parameter	Value
Gauge length	3 m
Sampling frequency	1000 Hz
Spatial sampling	0.5 m

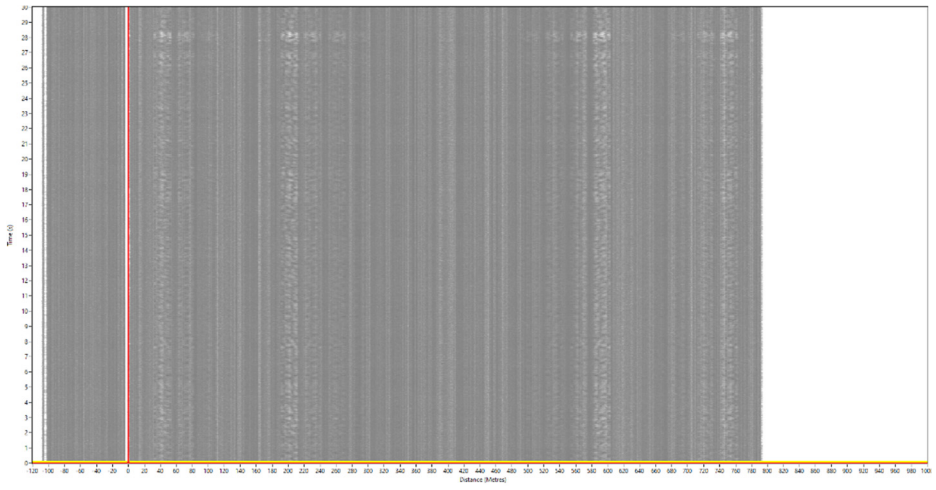

Figure 5 Example DAS data. The higher amplitude sections are the turnaround points as the cable cross the dam.

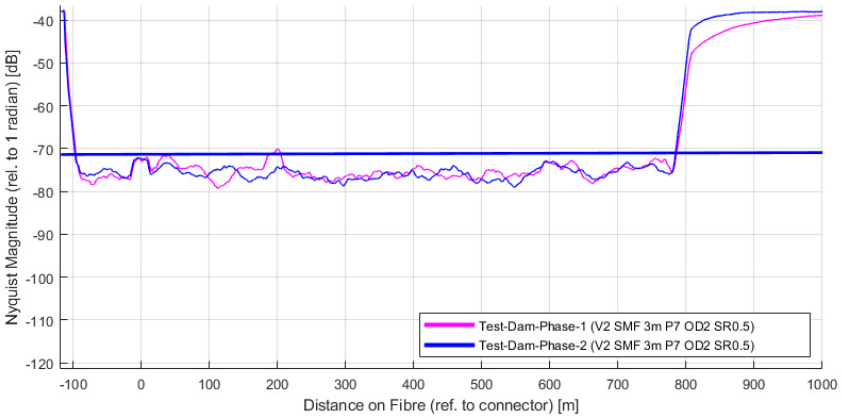

Figure 6 Theoretical noise floor for the Test Dam iDAS set-up (thick line) and the measured noise levels along the cable in Phase 1 (2020) and Phase 2 (2021) (thin lines).

3.6 RESERVOIR OPERATION AND OTHER MEASUREMENTS

The main filling of the dam up to the retention water level started on 4 May 2020 and the final level was reached in June 2020. This water level has since then been kept constant until the drawdown started in September 2021. Continuous measurements of the reservoir and air temperatures are made almost from the time before filling started.

DAS measurement started on 20 August 2021 and lasted until 11 November 2021. Measurements at constant high water level were achieved during 10 days, before the drawdown started in September 2021, with a first draw down of 1.5 m during seven days. This water level was kept constant for about 34 days (except for a lower dip for 9 days due to pumping failure). A further drawn down to 0.6 m was made for 6 days. This water level was kept during the remaining monitoring period. The water levels and temperature in air and water in the optical fibres during this period is shown in Figure 7.

a)

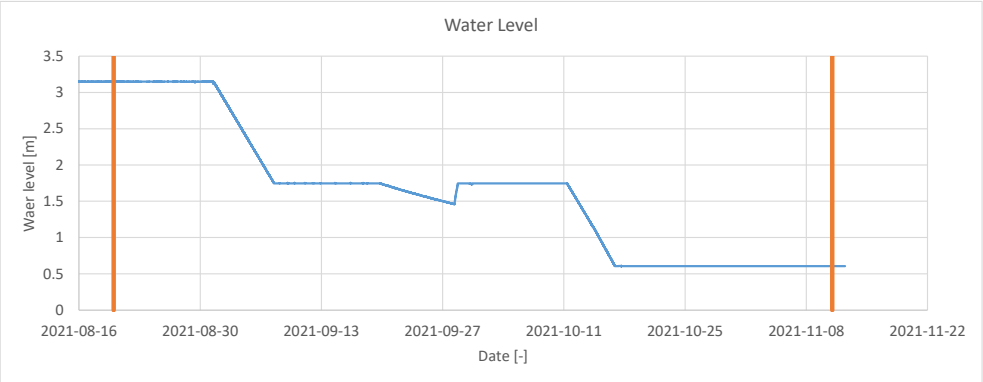

b)

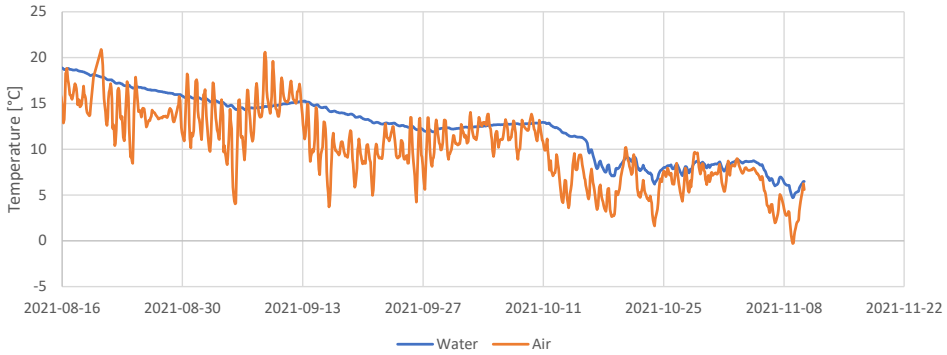

Figure 7 Water levels (a) and temperature in air and water (b), during the monitoring period (August 20 to November 11).

4 Effect of water level changes and dam defects on seismic velocities

4.1 SEISMIC VELOCITES IN DAMS

The velocity of seismic waves in a material is dependent on the physical properties of the medium. Therefore, measuring absolute seismic velocities can provide information on the composition of and heterogeneity within a dam through seismic imaging. With seismic monitoring over time, changes in seismic velocities can indicate changes in saturation or density/composition of dam material.

Compressional (P-) wave and shear (S-) wave velocities, V_P and V_S, respectively, in a medium are given by

$$V_P = \sqrt{\frac{K + {}^4/_3 \mu}{\rho}} \qquad \text{(Eqn. 1)},$$

$$V_S = \sqrt{{}^{\mu}/_{\rho}} \qquad \text{(Eqn. 2)},$$

where K is the bulk modulus, μ is the shear modulus and ϱ is the density. Here Rayleigh waves and coda waves are used to image and monitor the dam, respectively. Rayleigh waves are mainly influenced by V_S and only slightly by V_P. Coda waves are also more sensitive to V_S than V_P (the theoretical ratio between the potential shear and compressional energy at the free surface is $E_S/E_{Psurf} \approx 7.19$; Tregourès and van Tiggelen, 2002). Therefore, we only consider the theoretical effects of water level changes and defects on V_S, as our results will be mainly affected by changes in V_S.

The material properties of the dam could change for a variety of reasons. First, changes in fluid saturation, due to water level changes or precipitation, affect the density. The bulk density in fully saturated conditions of a material is given by

$$\rho = (1 - \varphi)\rho_s + \varphi\rho_f \qquad \text{(Eqn. 3)},$$

where ϱ_s is the density of the solid matrix, ϱ_f is the density of the pore fluid and φ is the porosity. In unsaturated conditions the porosity is replaced by the liquid volume fraction θ, and, assuming the density of air can be ignored,

$$\rho = (1 - \varphi)\rho_s + \theta\rho_f \qquad \text{(Eqn. 4)}.$$

So, where air is replaced by water the density increases, and the velocity decreases.

Understanding the relative effects is important for interpretation of the results. The replacement of air by water has a significant effect on the density. Other parameters factors affecting seismic velocities include compaction, load effects due to changes in water level and changes in weather (temperature and pressure). In this case these effects are considered to be less significant than the effect of water saturation and therefore we assess the expected effects on our results based on modelling of V_S variations with water saturation.

4.2 MODELLING SHEAR WAVE VELOCITY

The water content within the dam material is given by the material properties (porosity and saturation). The latter depends on the water level and will thus vary with time. This can be simulated using the sub-surface module of the finite-element software COMSOL Multiphysics, which solves saturated and un-saturated flow (i.e., the Richard equation). The model is made in 3D and has a width of 2 m.

We model the expected seismic response of the dam to changes in water level, first for the dam without defects and second with defects added. For the modelling we assume the parameters as given in Table 2. The material parameters for the material in the Test Dam have been provided based on tests. Value for the shear modules have only been provided for the core material. The same value is therefore assumed for the other parts of the dam. Actual water level and water temperature from the initial filling were used as transient boundary condition.

Table 2 Some key input data from Vattenfall used the simulations and estimated data in italic.

	Core	Filter Fine	Filter Coarse	Fill	Damage
Permeability k [m2]	5.32E-15	5.60E-12	2.70E-08	4.50E-08	3.38E-09
Porosity [%]	4.6%	12.6%	35.2%	35.7%	*20%*
Shear Module [MPa]	23	*23*	*23*	*23*	*23*

In the material properties it is assumed that minimum water content is 1%, which might not be perfectly correct in this case since the experimental dam is placed within a tent.

With the result from the simulations, we can better understand seismic shear velocity changes due to porosity, density, water content and other parameters in the different materials within the dam, as well as its changes with time. The above equations are used to produce velocity models of the dam.

4.2.1 Intact dam

Studies have shown that V_S generally decreases with increasing in fluid saturation. Therefore, an increase in water saturation, for example due to water level rise or precipitation/ snow melt, generally results in a decrease in S-wave velocity. This effect is seen in the Vs model for the intact dam at different water levels (Figure 8d) where the S-wave velocity is calculated based on the simulation result and Equation 4.

At a stationary water level, the groundwater level will be almost horizontal in the coarse fill and filter materials, while we will have a smooth water level drop in the core (Figure 8 c) the white line). At initial filling we can see that it takes time to obtain final degree of saturation as shown in (Figure 8 b and c. In the lowest part of the dam (below the downstream water level), we have full saturation, while the saturation above varies depending on the soil parameters and the water level variations. We can also see the different shape of the ground water level at initial filling and at decreasing water level when the core material is saturated (Figure 8a and d).

a)

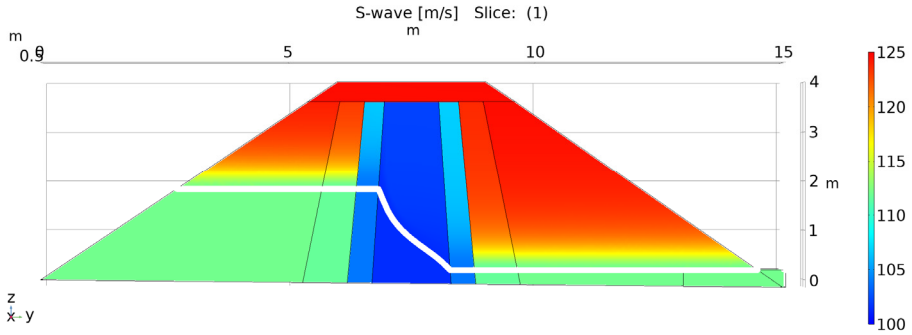

b)

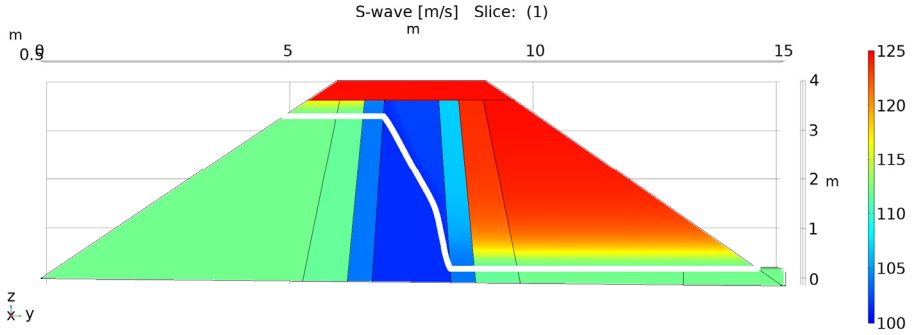

c)

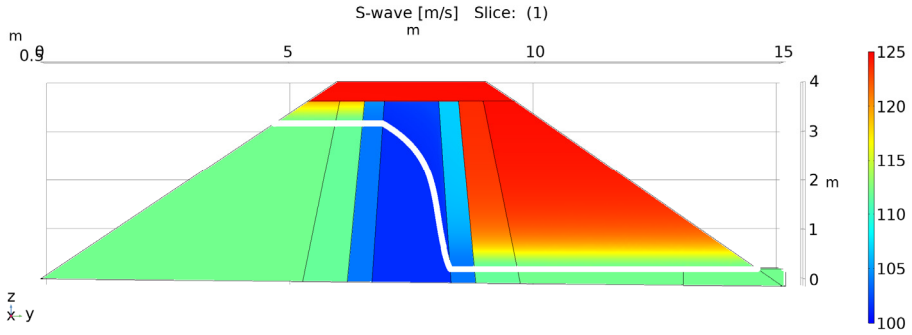

d)

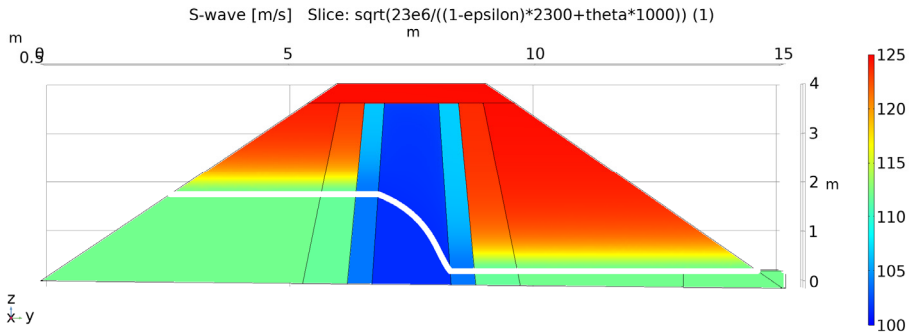

Figure 8. Modelled S-wave velocities at first filling at Phase 1 (a), and after reaching final level (b), level in 2021 during the second DAS measurements at beginning (c) and at second level at drawdown (d).

The temporal changes of the S-wave velocity during have been calculated for the selected points and some mean values are shown in Figure 9 . The change with the water levels is obvious, and significant decrease is seen first in the lowest points (L1-L7) and then followed by the points at the higher level (H1-H7) who are in the saturated area.

a)

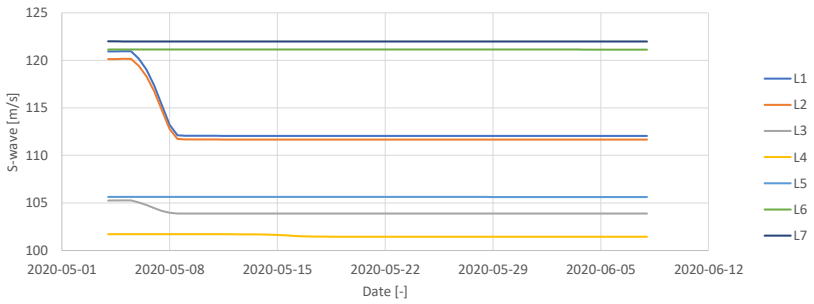

b)

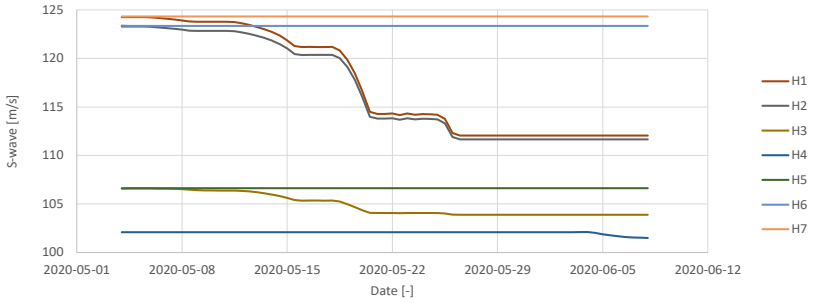

c)

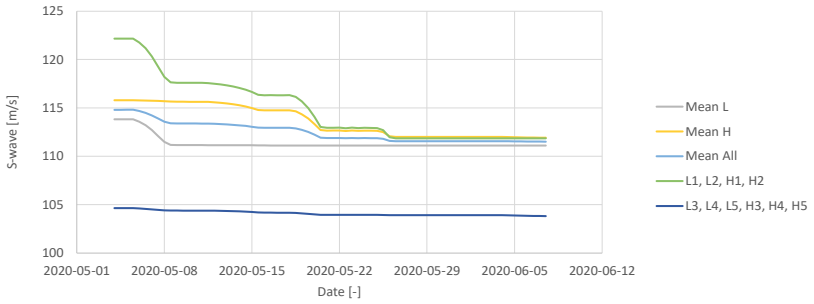

d)

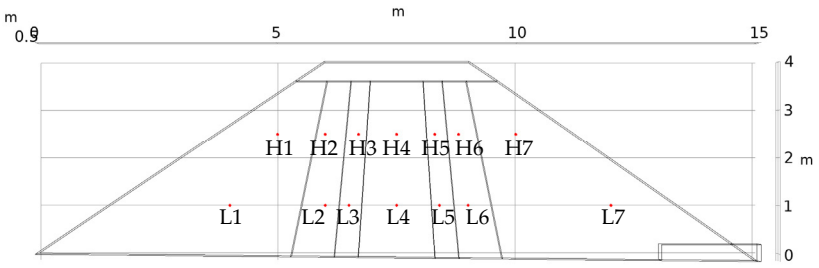

Figure 9 Calculated S-waves in points L1-L7 (a) and H1-H7 (b), and some mean values (c) during the first filling in 2000 (phase 1). The points H1-H7 and L1-L7 are shown in (d).

4.2.2 Horizontal permeable zone (Defect 2)

In addition to the overall effect of water level change on seismic velocity, the individual defects will respond differently. To enable an assessment of whether the effect of these defects is observed in the DAS data we selected modelling of one defect (Defect No 2) to provide an indication of the expected change in Vs of the defect material and the surrounding area to water level changes.

Some information of the defects has been given and defect 2 is 0.5 m wide and 0.1 m high and has the same material as the coarse filter (with a permeability about 500 000 times higher than the core). It is also surrounded by fine filter about 0.15 m in all directions. In the modelling we have replaced the two materials in the defect with one, where the permeability is about 60 000 higher than the core, and with a cross section of 0.8x0.4m. The porosity is assumed to 20% as a mean value for the two materials in the chosen area.

Figure 10 Defect 2 taken during construction (photo from Vattenfall)

The effect of a horizontal permeable zone in the core (Defect 2) are given in Figure 11. An increase in V_s compared to the intact dam is observed in the defects because the defect is composed of less dense material. Additionally, there is a more significant decrease in V_s downstream of the defect due to increased water saturation. This is also seen when plotting the velocity in some selected points for during the latest monitoring period (Figure 12). Changes is only clearly seen in the points in the core and fine filter in the lower line (L3, L4 and L5), where the porosity is changed. This will then change the S-wave velocities up to about 5 m/s compared with the velocities at an intact dam in the selected points, but only about 1 m/s when comparing the mean values.

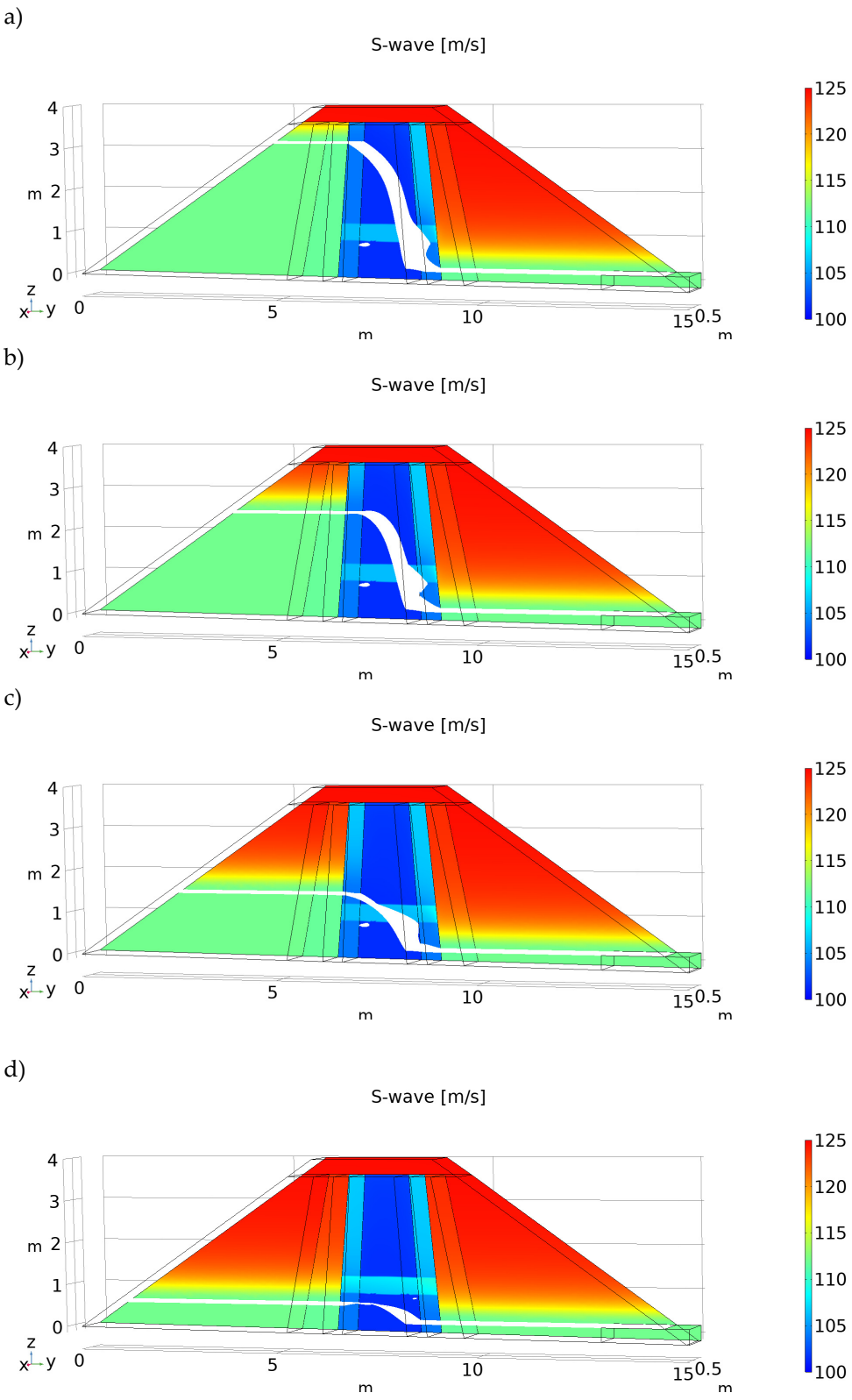

Figure 11. S-wave velocity model for a horizontal defect in the core for at different water levels.

The defect will change just slightly change the water pressure in the core, i.e. just minor changes in water content in the core. In points L3-L5 (located in downstream fine filter) we see a significant dependence of water level changes. These changes may be seen by the measurements, but the information may not allow to estimate the depth of the defect.

a)

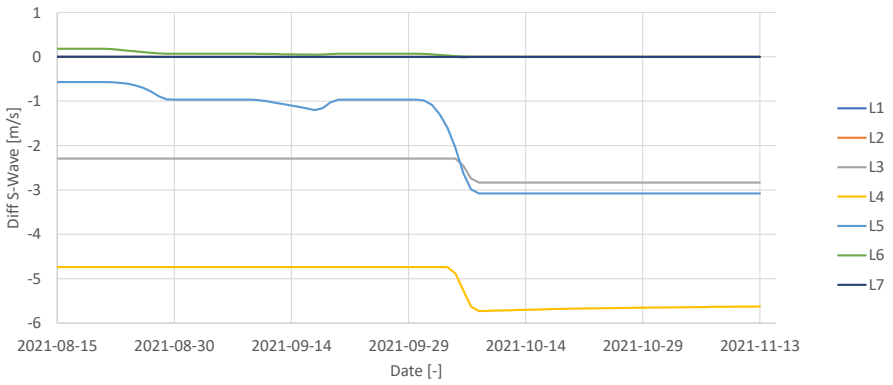

b)

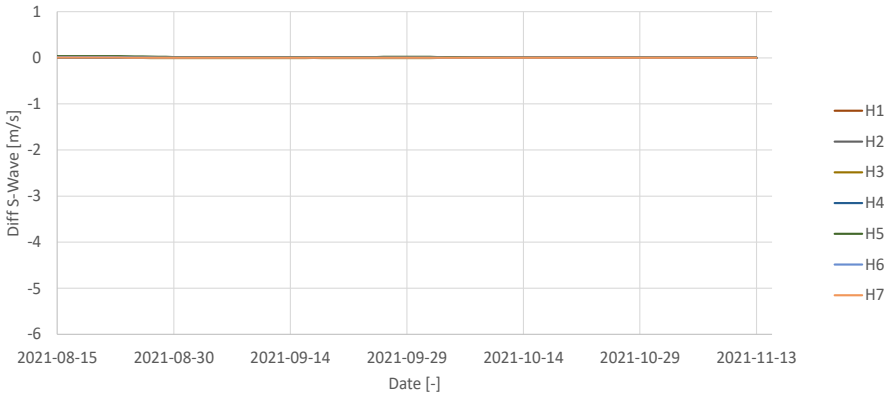

c)

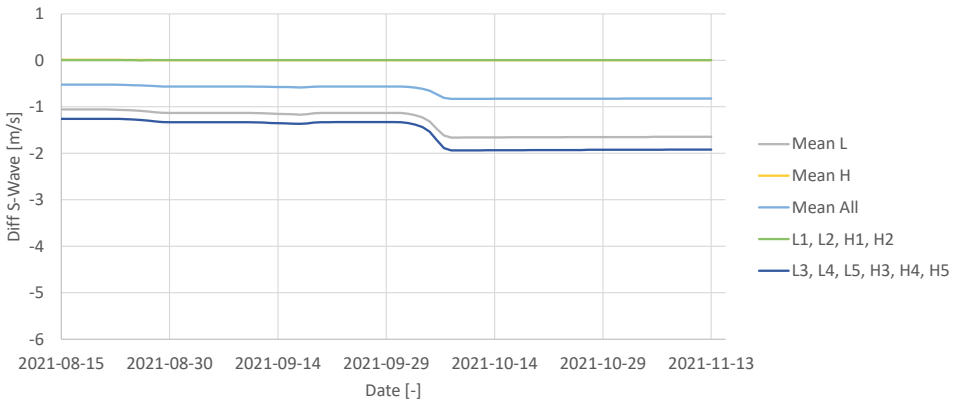

Figure 12 S-wave velocity difference between intact dam and dam with defect 2 in points L1-L7 (a) and H1-H7 (b), and some mean values (c) at water levels during Phase 2. The location of the points H1-H7 and L1-L7 are shown in Figure 9(d).

4.3 CONCLUDING REMARKS/GUIDELINE FOR INTERPRETRATION

The expected observations of absolute and variations in V_s with water level changes are given in Table 3. These are supported by the modelling results given above for defect 2, but also defect 3, 5 and 6 will increase the permeability with larger grained and less dense material. All these defects will therefore behave similar with higher V_s than the surrounding medium in a steady state. They will also respond quicker (with a lower velocity when saturated) to changes in water level because the defects will saturate/drain quicker. Any increase in permeability will increase the rate of change in saturation of material downstream of the defect. The solid block defects (1 and 4) are expected to have higher Vs than the surrounding medium but not be affected by water level changes since they have very low porosity and permeability.

Table 3 The expected effect of the defects on seismic velocities within the defect the surrounding medium with changes in water level

	Defect	**Steady state drained V_s within defect compared to surrounding**	**V_s change in defect with filling**	**Effect on V_s downstream of defect with filling/draining**
1	Wooden cube (pine)	Higher (~1.5 km/s)	Very slow / no change	Little effect
2	Horizontal permeable zone in core	Higher than core material	Decrease	Decrease with filling/increase with draining.
3	Vertically loose zone	Higher	Decrease	Decrease with filling/increase with draining.
4	Concrete block	Higher (~1.9km/s)	No change	No change
5	Horizontal permeable zone at side	Higher	Decrease	Change in velocity faster than surrounding medium both in defect & downstream. Decrease in Vs downstream with filling/increase with draining.
6	Filter defect upstream	Higher	Decrease	No significant effect expected compared to surroundings in steady state. Any velocity changes would initially occur quicker than surrounding areas.

5 ANI monitoring and imaging methods

5.1 INTRODUCTION

Passive seismic methods make use of the natural or anthropogenic noise. These passive methods do not require direct human intervention, resulting in cost savings compared to active methods. Data can be recorded on-demand, independent of weather conditions or time of day, and can be performed continuously if required. The recorded signal provides information on the velocity and amplitude of the seismic waves in the dam, and these can then be related to material properties (cf. Chapter 4).

Given the advantages of passive seismic methods, the feasibility of using ANI in combination with DAS measurements to image and monitor seismic velocity variations in the dam, is tested at different water levels.

Measurement during first filling in spring 2020 (Phase 1) was performed and evaluated as described in the previous report as mentioned above. The water level was then kept constant at high water level, until it was lowered in stages in Autumn 2021 (Phase 2). For this second phase of tests, we used intra-fibre and inter-fibre correlations along the crest, USL2 and DSL3 fibres to measure changes in velocity over the 81 days of recording using an improved DAS-interrogator.

5.2 AMBIENT NOISE INTERFEROMETRY (ANI)

ANI makes use of naturally occurring and anthropogenic background noise to calculate seismic velocities and hence image the subsurface. By **cross-correlating** noise records between two sensors, it is possible to reconstruct the Earth's response as if one sensor were a seismic **source** and the other a **receiver**. Thus, a seismogram is produced. The output from ANI are estimates of seismic wave velocities in the dam/subsurface, with the resolution and depth of investigation dependent on the type of waves investigated and the available frequency bands. Seismic velocities give information on the characteristics of material in the dam/subsurface. For the case of surface waves, lower frequency studies provide information on deeper structures. Additionally, by studying seismic velocity changes through time, it may be possible to detect changes in water saturation or structure (for a detailed description of ANI principle, please refer to the Phase 1 report and references therein).

5.3 ANI DAS MEASUREMENTS

The development of capabilities to use ANI with DAS data has significant advantages over traditional methods which use expensive active source seismic surveys and point sensors which require significant manpower to deploy for a large survey. ANI is a passive technique which means the instrumentation is left to record for a given amount of time without needing personnel present. Fibres can be permanently deployed so data can be collected continuously or as required. The distributed nature of DAS recordings and the potential DAS provides to use cables up to 40 km-long means that information is available over large distances and down to sub-metre scales, if required.

DAS data is similar to strainmeter data. They are mostly sensitive to along-fibre travelling waves which deform the fibre longitudinally. P-wave travelling along the fibre are well recorded with DAS. S-waves need to travel with an angle of 45 degrees from the fibre to obtain the maximum sensitivity (same for Love waves, Figure 13). Rayleigh waves are also well recorded when they travel in a direction parallel to the fibre (Zhan, 2020). Studies have shown that DAS can have a large dynamic range with a flat frequency response for a wide frequency range as long as the gauge length is smaller than the measured wavelength of the waves. This will limit some of our applications at high frequency. The self-noise of DAS is usually comparable to the one of standard short-period geophones (Zhan, 2020).

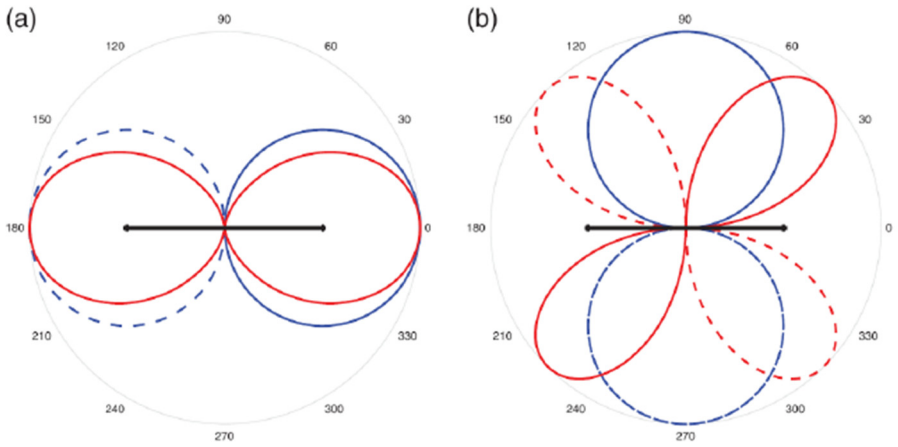

Figure 13 (a) Red lines show directional sensitivity of DAS, or linear strainmeter in general, to P wave for a straight fibre section aligned along the horizonal axis (black lines). Solid and dashed lines mean positive and negative, respectively. The directional sensitivity of a conventional seismometer's horizontal component is shown in blue lines as references. (b) Same as (a) but for S waves. Modified from Zhan (2020).

The spectral analysis of data recorded during the two phases shows the level of ambient noise and instrumental noise (Figure 14). The DAS interrogator used during Phase 2 shows a lower instrumental noise level than the interrogator used during Phase 1. An interrogator with greater sensitivity (lower noise floor) facilitates the recording of smaller amplitude signals. For ambient noise analysis a shorter time period of recording would be needed to obtain good SNR data.

This is particularly visible between 0.1 to 3 Hz where the mean level of instrumental noise is of about -15 dB during Phase 1, and around -20 dB during Phase 2. This difference enabled the detection of the second microseismic peak at 0.2 Hz during Phase 2. If we suppose that the level of ambient noise remained stable between the two phases, the spectrograms indicate that the Phase 2 interrogator has a higher sensitivity than the Phase 1 interrogator. For the same noise level, the dynamic range of Phase 2 data is 15 dB larger than Phase 1 data.

In this preliminary analysis, we noted also a 3 day-long gap in the data at the beginning of October.

The ambient noise level is assumed to be the same since the recordings in Phase 1 and Phase 2 are made at exactly the same location and no major change in noise sources is observed in the data. Changes in noise sources could make the technique

more or less sensitive at the frequency of the noise source. Strong noise source off-line from the cable create apparent velocity effects that would need to be considered/corrected for.

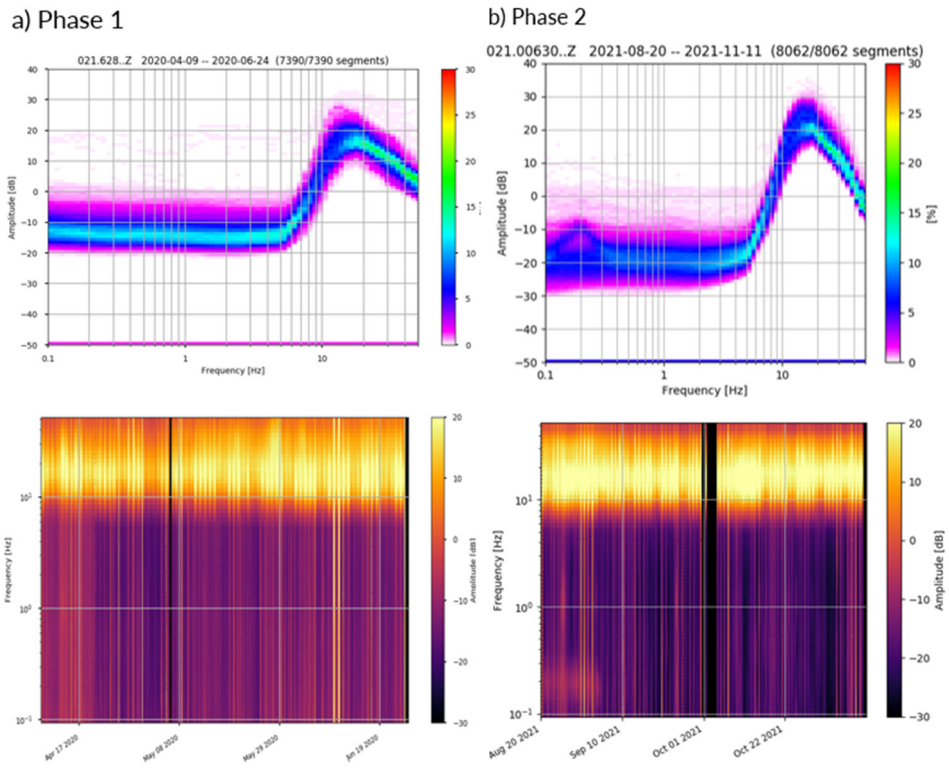

Figure 14 Spectral analysis of data recording at a channel along the crest fibre during Phase 1 and Phase 2. Top: Probabilistic representation of spectrograms computed on 1 hour-long time segments, represented at the bottom along recording time.

5.4 ANI MONITORING METHODOLOGY

We use coda-wave interferometry to measure the relative seismic velocity changes within the dam for the whole monitoring period (for a detailed description of the method, please refer to the Phase 1 report, Johansson et al., 2020).

The monitoring application is performed on 35 channel pairs with similar inter-channel distances sampled along the dam every 0.5 m along the crest fibre. Stable results are obtained with a temporal resolution of 30 minutes.

The analysis starts with a careful selection of a "Reference", a frequency band of analysis and a lag time over which the stretching method will be applied.

The reference correlation should be representative of an average state of the monitored medium. We calculate the mean of all correlations during the most stable period of recording (21^{rst} -26th August). The correlation coefficients between the mean correlation and the individual ones are then computed and the final "Reference" is taken as the average of all correlations having a correlation coefficient >=0.7 with the mean correlation. This procedure allowed us to reject the correlations that are corrupted and not representative of the medium state.

Figure 15 shows a set of correlations for the pair of channels 021.625-021.615, together with the corresponding average correlogram. Velocity variations are clearly observed in the data during periods of water drainage highlighted in grey. These variations are observed from 15 to about 25 Hz. The frequency band will determine the type of wave used for the monitoring and its sensitivity to changes in the medium. For our analysis the frequency has to be high enough so that the wavelength is short enough for the wave to be mostly sensitive to the dam in the surroundings of the two sensors used for the correlation. After trial-and-error, the frequency band 15-27 Hz is found to be the most suitable to measure velocity changes. Above 27 Hz, measurements of velocity variations are difficult because of the noisy nature of the signal.

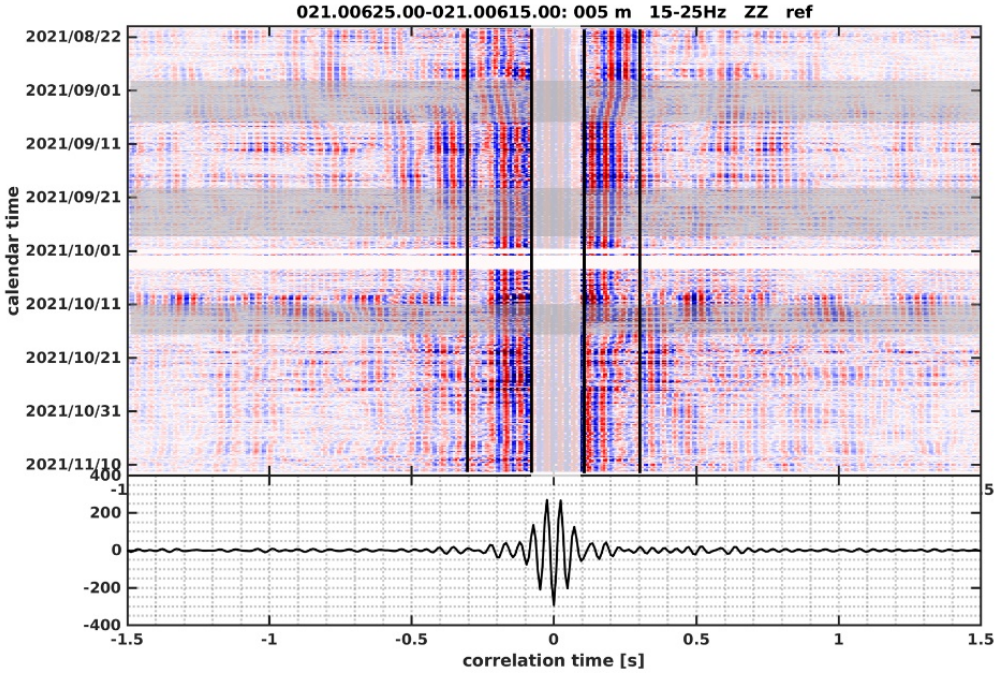

Figure 15 Individual 30-min correlations ordered according to the calendar time. The time bounded by the black lines indicates the lag-times used for the monitoring measurements. Grey zones indicate periods of water level changes. The average correlation over the whole recording duration is represented at the bottom.

The time window determines the type of wave (direct or scattered) used for the monitoring. It also determines the volume sampled by the wave and therefore the spatial resolution of the monitoring results. The later in the coda of the correlation the window is, the longer the wave has stayed in the medium to sample and accumulate its changes. Longer lag-time are more sensitive to changes but scattering and attenuation decrease the amplitude and the quality of the signal. To choose the proper window we balance this trade-off. The coda windows are chosen to be symmetrical around the zero lag-time. After trial-and-error, the window 0.1-0.3 s on both side of the correlations is chosen.

5.5 ANI IMAGING METHODOLOGY

For this second phase, timelapse imaging was attempted using eikonal tomography. Parameters were tuned over 5 days-long stack of correlations at 4 different water level stages before performing a batch computation of the one-day

time lapse tomography (for a detailed description of the eikonal tomography method, please refer to the phase 1 report).

The imaging method is performed on all channel pairs sorted in 40 virtual shot gathers (i.e. each channel taken as a virtual source versus all the other channels taken as virtual receivers). The analysis starts with a careful selection of a time window, a wavelength window, and a frequency band of analysis over which the eikonal method will be applied.

The minimum wavelength is set to avoid near source effect. On the example below (Figure 16), arrivals at distance lower than 4 m are muted in order to avoid measuring the "flat" arrivals. The maximum wavelength is chosen to select only high signal to nose ratio (SNR) correlations. The SNR decreases with inter-channel distance. As the dam length is short, there is no SNR decrease. The maximum wavelength is set to exceed the length of the dam.

The time widow is chosen to frame the main arrival between 0 and 0.1s at 0 m, and 0.00 to 0.2 s at 20 m of distance. At long distance, reflection arrivals against the dam's end interfere below that window.

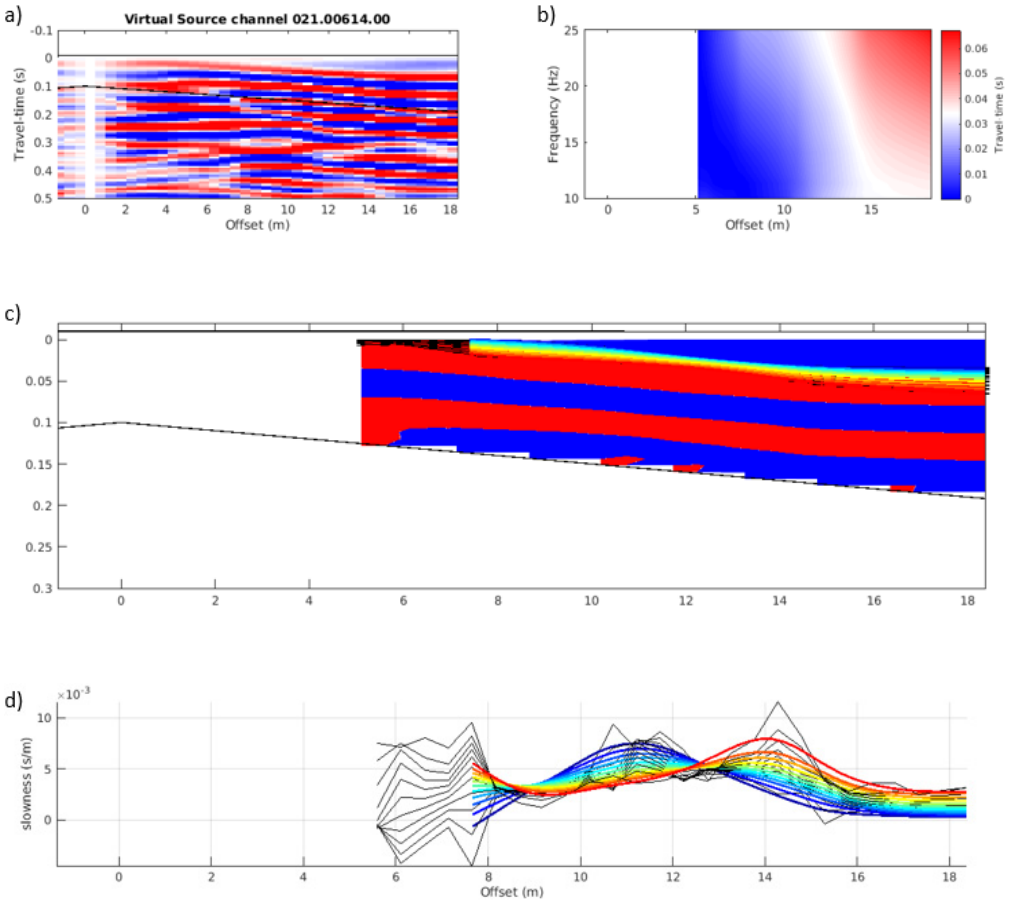

Figure 16 Example of travel-time measurement and eikonal tomography for sensor 614 taken as the virtual source: a) virtual shot gather bandpass filtered between [10-25] Hz; b) Fourier transform c) travel-time measurements superimposed onto muted shot gather; Colored lines (red to blue for low to high frequency) represent smoothed travel-time measurements and black lines raw measurements with their error bar. d) Gradient of the travel time curves equal to the slowness; Colored lines represent smoothed slowness and black lines raw slowness.

The frequency band is chosen to avoid spatial aliasing at high frequency. The low frequency bound is defined by the minimum wavelength which can be reconstructed in the range of interstation distance analyzed. Travel-time measurements were made between 10 to 25 Hz.

Travel time measurements (in black on Figure 16c) are smoothed to stabilize the computation of the gradient which provides the slowness of the arrival (Figure 16d). Measurements are controlled by a simple quality check to remove outliers – velocities outside [50 - 1500] m/s interval -- and compute statistics. The final phase velocity dispersion curve and its error bar corresponds to the average of all measurements at a point along the dam and its standard deviation.

Each local dispersion curve is inverted in the second processing step (Figure 17). The parametrization was adapted to the larger range of velocity measured in phase 2 compared to phase 1 (Table 4).

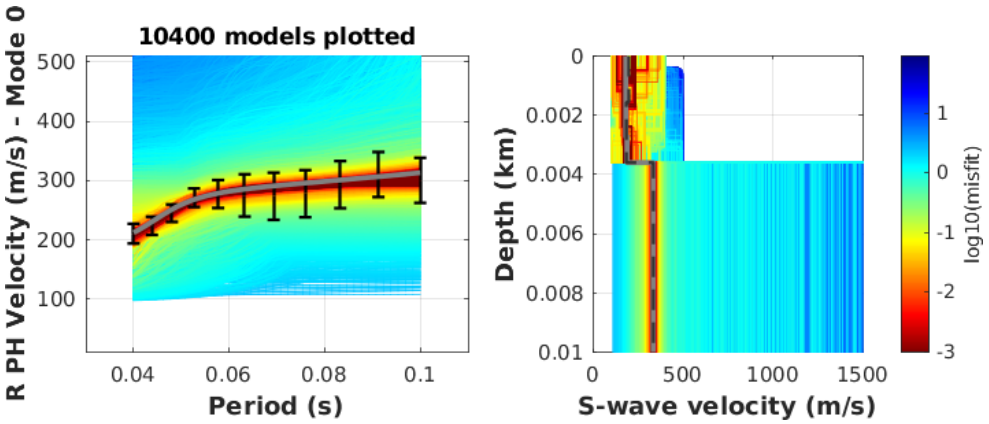

Figure 17 Example of local inversion point: to the left, in black the dispersion measurements; to the right the Vs models. The bold grey curves represent the best model over all the model tested represented by the thin colored lines. The colors indicate the misfit of model tested. The range of tested Vs model is defined by the parametrization described in Table 4.

Table 4 Model space parametrization.

Parameter	Description	Min	Max
d1	Thickness of the first layer * dam height	0.1	0.9
v1	Velocity in the first layer	100	400
v2	Velocity in the 2nd layer	100	500
v3	Velocity in the third layer below the dam	1.0	10.0
vhs	Velocity in the halfspace * v3	0.9	1.3

Imaging and timelapse was tested on different amount of correlation stacking, from 1 day to 5 days. Stable results were obtained from 5 days of stacking. The timelapse was performed at a step of one day over a stacking window of 5 days.

5.6 INTER-CABLE CROSS-CORRELATIONS FOR IMAGING & MONITORING

Cross-correlations across the dam were computed between fibre sections CREST, USL2 and DSL3 for the entire duration of acquisition.

The preliminary analysis consisted in a visual inspection of a series of shot gathers in order to better understand the type of waves retrieved (direct or reflected waves; body or surface waves, Figure 18a).

We also measured the relative velocity variations in between pairs of channels at the same section along the dam (Figure 18b) in order to analyze only the same ray path directions.

a)

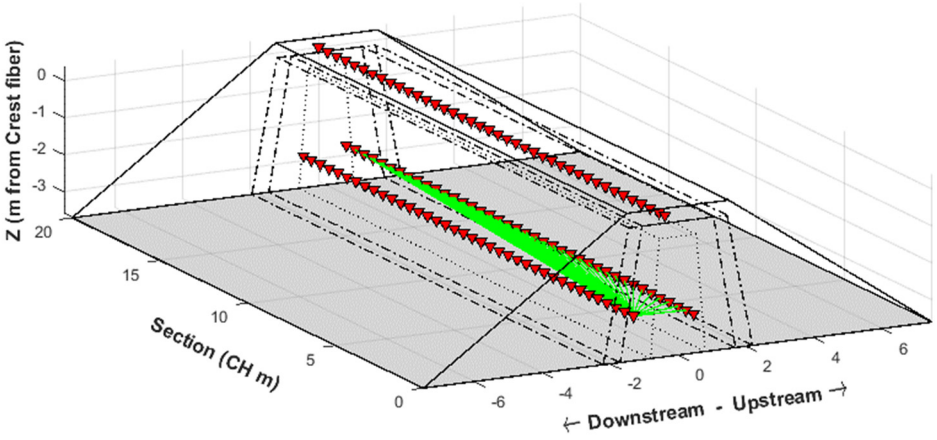

b)

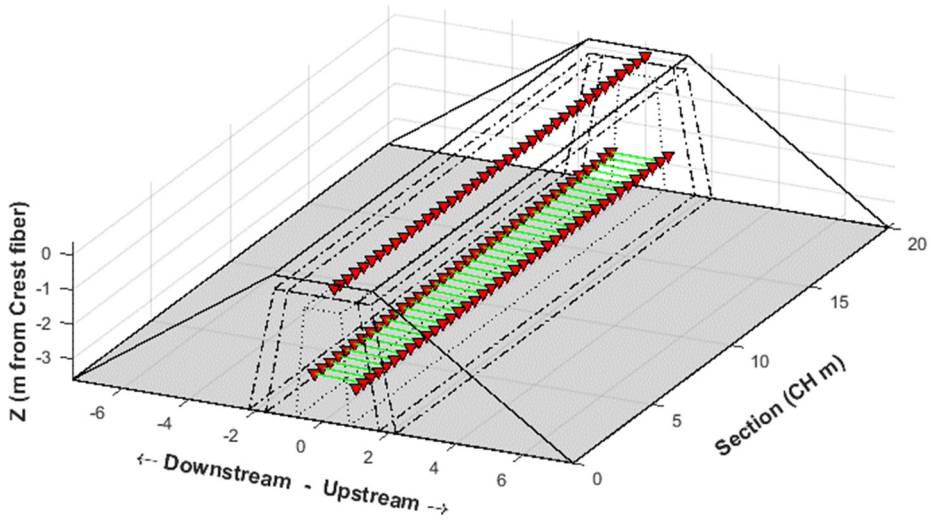

Figure 18. USL2 and DSL3 locations in the dam. Red triangles represent channels used to compute inter-fibre correlations. Correlation paths in green represented on virtual shot gather (a) and monitoring analysis (b).

6 Evaluation of measurements at decreasing water levels in 2021 (Phase 2)

6.1 MONITORING

Figure 19 shows the average travel time variations (black line) together with water temperature (dotted red line), air temperature (red line) and water level measurements (blue line), for the whole recording duration. Several successive gaps in the data between the 1rst to 5th October are highlighted in grey. There are three periods of significant travel-time decrease (highlighted in blue), accumulating a total of about 8% of travel-time change. The first and second periods correspond to water drainage periods. The third period starts a couple of day after the drainage restart and extends over 10 days after.

The travel-times displays consecutive step-like decreases correlated with the drainage of the basin. These travel-time decrease steps seem to have a lower amplitude each time there is a water drainage. Daily variations of the travel-time can be correlated with night/day temperature change. At a larger scale, there is no straightforward correlation of the travel-time with the water or air temperature variations.

Spatially, along the dam chainage, some part of the dam sustained more than 20% of velocity increase while draining water (Figure 20). This is observed at Section 9 and 13 m. Conversely, some parts of the dam are not affected by the water change. This is especially clear around Section 11 m.

The uncertainty on the measurements is constant over the dam chainage, around 1.8%.

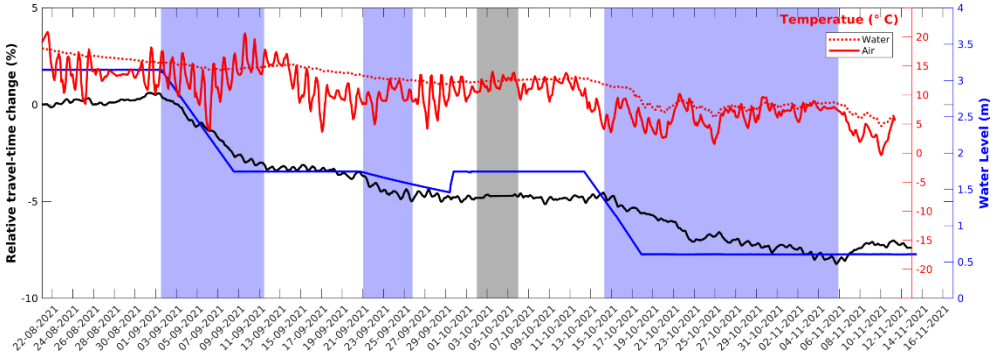

Figure 19 average travel time variations (black line) together with water temperature (dotted red line), air temperature (red line) and water level measurements (blue line), for the second recording period.

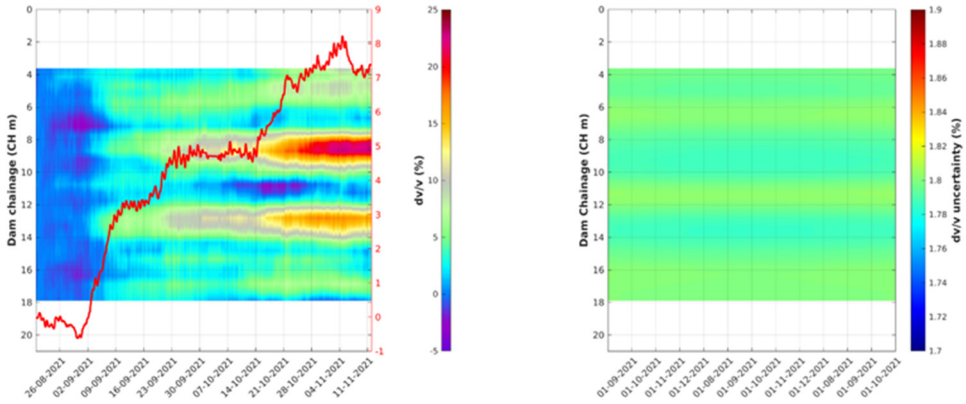

Figure 20 to the left, dv/v measurements along the dam chainage, to the right the uncertainty on dv/v measurements. The red curve represents the average of dv/v.

6.2 IMAGING USING CREST CABLE

In this report are presented the models depicting the velocity state of the dam before and after the water emptying (Figure 21). The timelapse images can be provided separately in a video format, but results are summarized in Figure 22 and Figure 24 hereafter.

6.2.1 Phase velocity dispersion results

Phase velocity dispersion values were obtained by the eikonal method. Figure 21 displays the dispersion measurements at two different stages of water level. At the first stage, velocities are low, with an average around 250 m/s. The same high velocity zone as in Phase 1 is found at the end of the dam. After the drainage, the dispersion measurements indicate an increase of velocity of 57 m/s in average. Velocity contrasts are enhanced, with velocity reaching up to 450 m/s in two high velocity zones at 7 and 11 m of section.

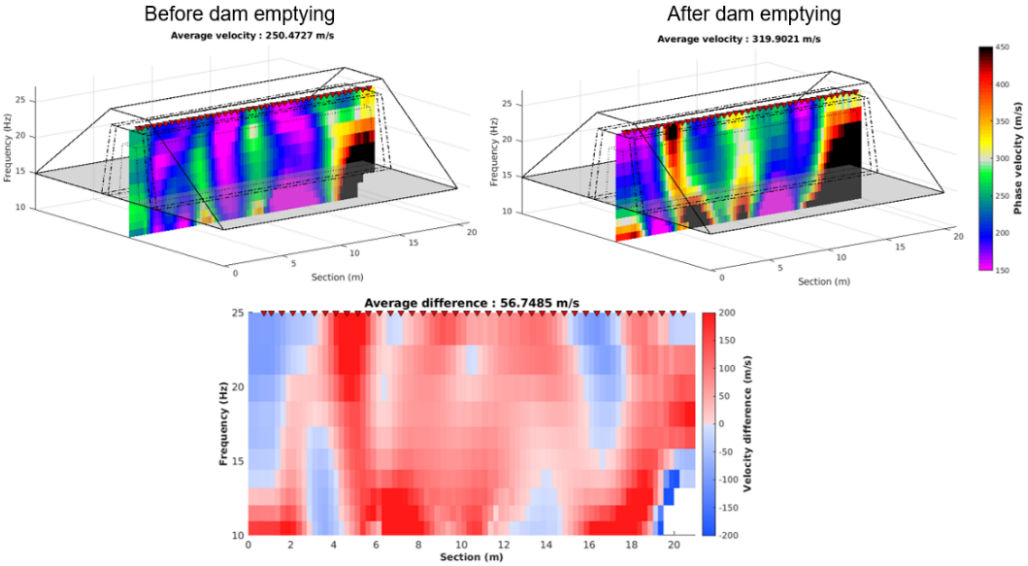

Figure 21 Dispersion measurements before and after dam emptying, and the difference between both dispersion sections. Red triangles represent the channels used. The same trend is observed in the average.

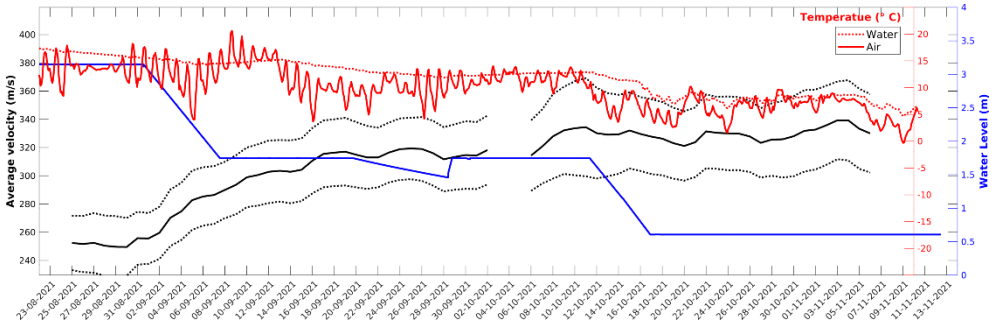

Figure 22 Average velocity evolution of dam's core crest in the frequency interval [10 - 25] Hz in black together with its uncertainty (dotted black lines). The evolution is compared to the evolution of water level (blue line) and of the temperature of water and air (red curves) along the recording duration.

6.2.2 S-wave velocity models

The dispersion measurements were inverted to obtain models of S-wave velocities (Vs) versus depth at the two different stages of water level (Figure 23). Timelapse models were also compute for all dispersion measurements with a one-day step (results in video format attached to this report and summarized on Figure 24). The models obtained are well resolved between 1.3 m and 8.5 m depth. Velocities in the dam range between 100 to 911 m/s, and velocities below the dam range between 150 to 1400 m/s. Before dam emptying several individual low velocity zones are found in the dam wall. After the dam emptying the low velocity zones joined, drawing three oblique bands connecting the base and top of the dam.

The velocity difference panels highlight the location of the velocity changes (see bottom of Figure 23). The main velocity change is located at the base of the dam between 6 and 8 CHm and between 16 and 18 CHm. These zones sustained a strong increase of velocity.

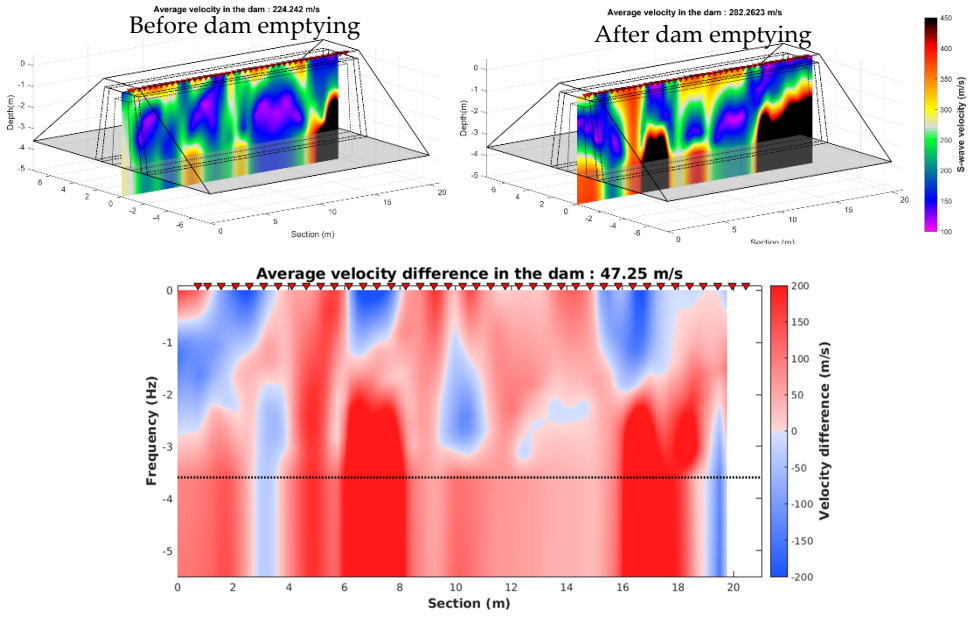

Figure 23 Vs models of the dam before and after dam emptying, and the difference between both models. Red triangles represent the channels used. Average values in titles correspond to average Vs in the dam wall, only.

Average velocities in the dam are less stable after inversion than the dispersion measurements (Figure 24). The trend is also slightly different compared to dispersion measurements, when only the dam is considered (Figure 24, black line). The medium below the dam seems more affected by the water level change (Figure 24, grey line) than the dam wall and sustained the largest changes of properties.

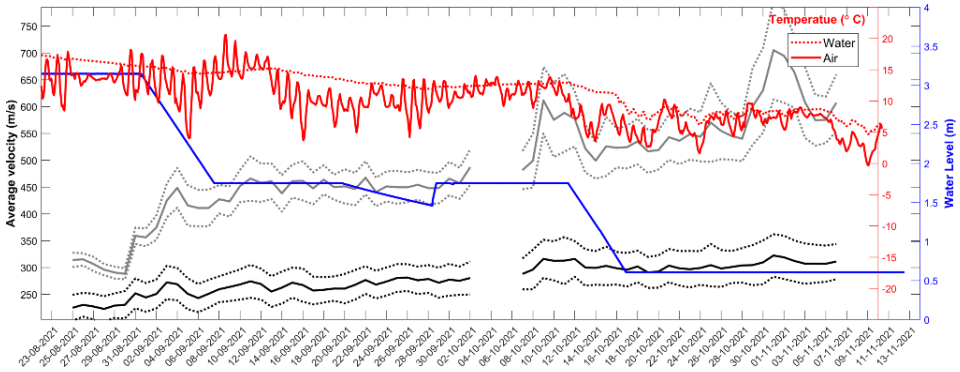

Figure 24 Average velocity evolution in the dam wall (0-3.6m depth) in black together with its uncertainty (dotted black lines). Average velocity evolution below the dam wall (3.6 - 5.5 m depth) in grey together with its uncertainty (dotted grey lines). The evolution is compared to the evolution of water level (blue line) and of the temperature of water and air (red curves) along the recording duration.

6.2.3 Comparison with monitoring results

The comparison of V_S models with monitoring results is not straightforward. Indeed, monitoring results are computed over 5 m distant pairs of channels and the results are attributed to the center channel. For a better comparison with Vs models, the monitoring results would require a regionalization step, in order to obtain local values. This step is not necessary when working at larger scale but in this case, it would help reconcile both results.

The comparison of averaged results shows that the monitoring method enables to detect very small velocity changes, with a very good accuracy like velocity variations due to air temperature change. The imaging method is less accurate both in term of time and velocity. Its advantage is the spatial information. Thus, the combination of both methods provides the location of the velocity changes.

The first drainage period led to strong changes in the core of the dam, as imaged, while the second and third drainage period generated the strongest velocity changes outside of the sensitivity area of the wave used for imaging. The coda wave monitoring samples a larger volume than the imaging with direct waves because the technique uses scattered waves.

a)

b)

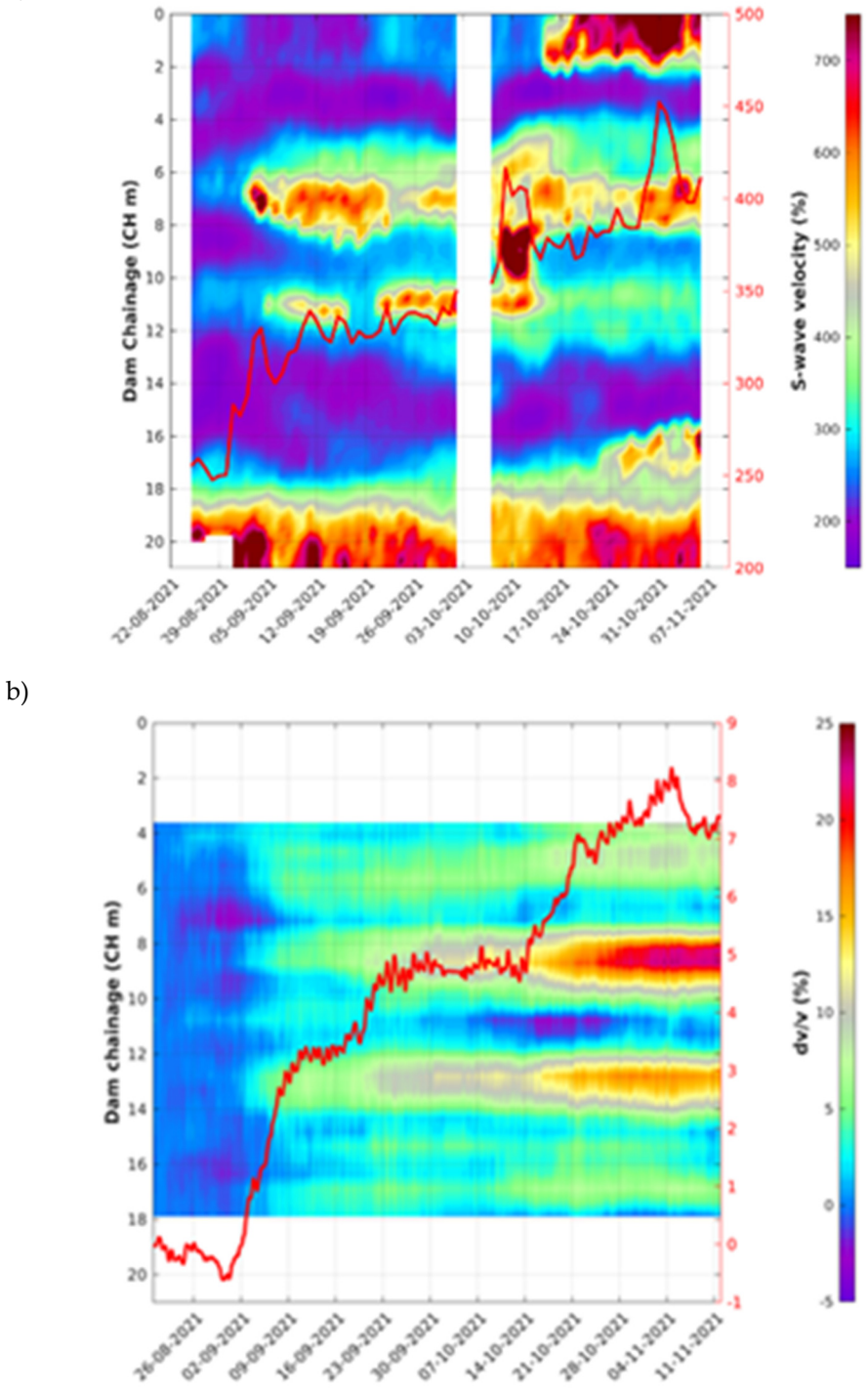

Figure 25 a) The heat map represents the average of timelapse Vs models. The red curve represents the average velocity measured in the dam wall. b) Monitoring results from Figure 20 plotted again for comparison.

6.3 PRELIMINARY INTER-CABLE IMAGING RESULTS

6.3.1 Results

Stacking cross-correlations over the entire recording duration enhanced the arrivals of waves propagating inside the dam. A first direct wave arrival with an average velocity of about 250 m/s is reconstructed on the acausal part of the correlations (red dotted line on Figure 26). Because of the DAS directional sensitivity and the relative position of the two fibre cables, this arrival is interpreted as a Rayleigh surface wave travelling in the direction of the dam. The second arrival on the acausal part, which is the dominant one in the stack section, is most likely a reflection because of its hyperbolic shape. The later arrivals are also reflections, either multiple reflections or reflections on more distant interfaces. Some earlier arrivals between 12 and 20 CH m might corresponds to Love waves or reflected body waves. The multiple reflections interfering with the direct arrivals are expected in such a 3D structure bounded by free surfaces and sharp vertical velocity contrast at dam's extremity. However, they don't provide information on the dam core.

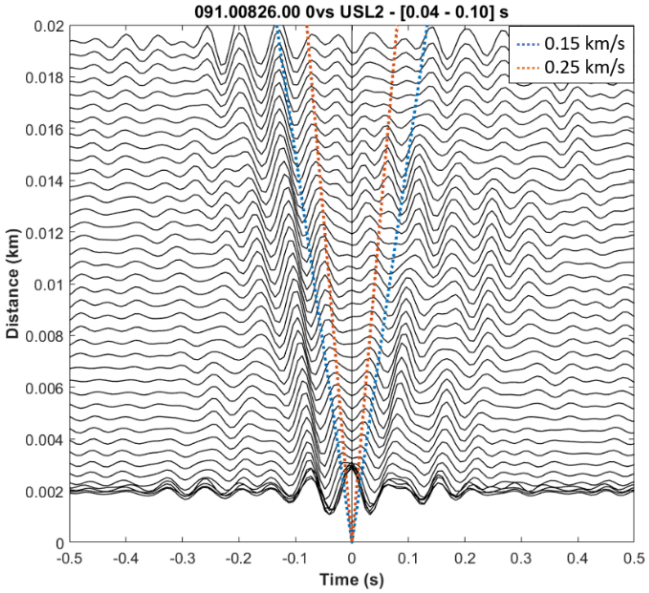

Figure 26: Virtual shot gather of noise cross-correlations between USL2 et DSL3. Traces are bandpass filtered in between 10 and 25 Hz. Colored dotted lines highlight iso-velocity values.

At short inter-channel distances, the strong amplitude peak at 0 s lag time corresponds to a Rayleigh wave travelling inside the dam, in the same direction as the fibre and recorded simultaneously by both channels. Any delay of this arrival may indicate either a velocity anomaly, or a wavefront travelling with a different angle.

We further analysed this short inter-channel distances, which correspond to channels face to face on both sides of the dam core (Figure 27). Correlation coefficients (CCF) reflect variation of velocities compared to average velocity of cross-correlations. CCF were computed for a series of 5 Hz frequency bands and for a wide frequency band: [1-26] Hz. Only the most relevant frequency band is showed in this report (Figure 27).

CCF was computed at two different stages of water emptying. On average, the CCF increases as the water level decreases, indicating a medium that evolves toward the average value, in other words the dam core getting more homogeneous in term of seismic velocities as water level decreases.

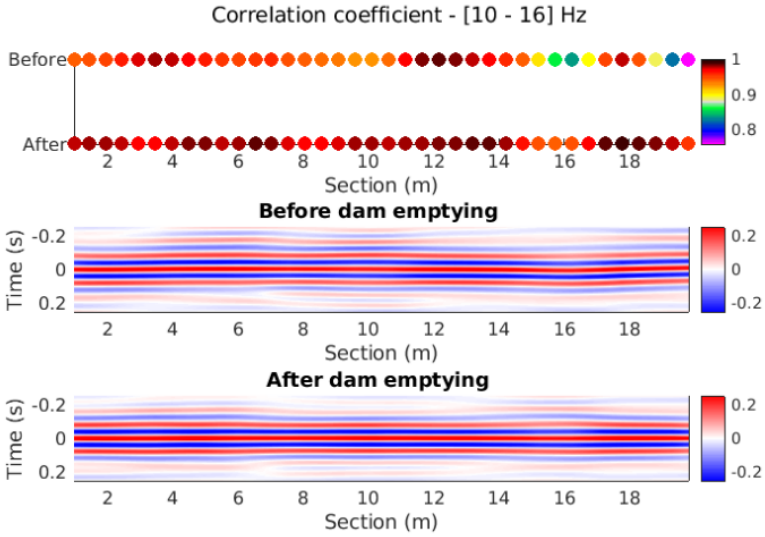

Figure 27 Correlation coefficient between average and individual correlations represented by colored circle computed before and after dam emptying on data represented just below. Sections used to compute the correlation coefficient filtered between 10-16 Hz. The correlation coefficient is lower before dam emptying than after, indicating stronger velocity variations compared to the average than after dam emptying.

Between USL2 and DSL3 cables, located at same depth in the dam wall, we were able also to monitor the variations of travel time over time in the coda (Figure 28). The total relative velocity change is an order of magnitude lower than the results obtained along the crest cable. Cross-correlations between USL2 and CREST, and between DSL3 and CREST were also computed but no significative velocity change was observed.

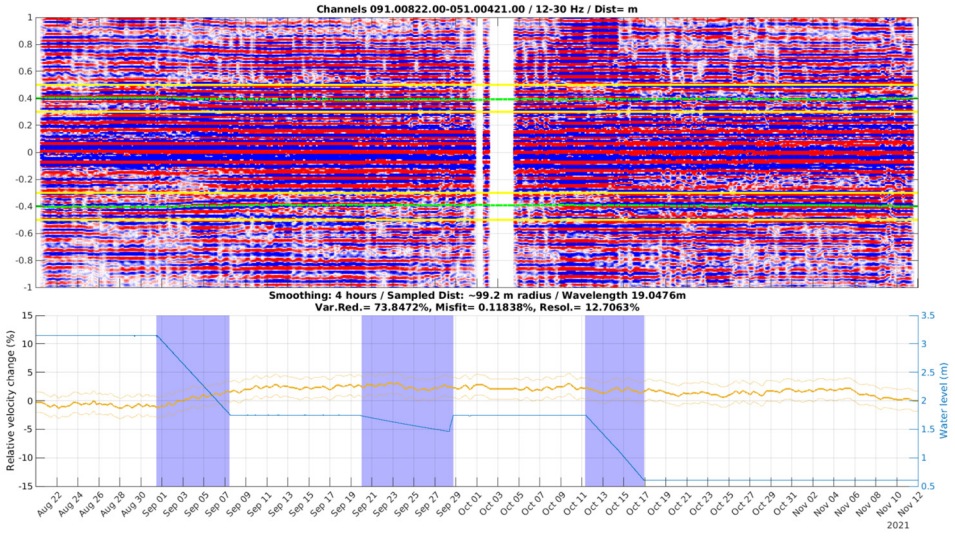

Figure 28: Example of monitoring results for a pair of channels on USL2 and DSL3 cables located at 3 CH m. The top panel represents correlations in amplitude vs time. Yellow lines bound the symmetrical intervals of lag time on which the relative velocity changes is measured. Green lines represent the travel time measured. On the bottom graph, relative velocity changes are plotted in yellow together their uncertainty (dotted yellow line) and the water level in blue.

6.3.2 Discussion

Preliminary analysis of inter-fiber correlations showed that we mainly detected reflections and only weak direct and coda waves. Imaging technique is using direct waves, and monitoring technique is using coda waves. No existing technique is using reflected surface waves.

Because of the 1D directional sensitivity of DAS systems, correlations between different cables require careful consideration of the relationship with geometry of wave propagation in such a 3D structure as earthen dams.

To simplify the problem, we can consider that waves are travelling along the dam length, parallel to the fibers. According to the theory, the direct surface wave on inter-fibre correlations should be the same wavefront than the one measured along the crest cable but recorded under a different angle. Given the 1D DAS sensitivity, at 90° angle to the fiber, i.e. for correlations between face-to-face channels, no signal should be reconstructed except the peak at 0s of lag time corresponding the wavefronts hitting simultaneously both channels. Here we observed some reflections. Moreover, Rayleigh waves should be recorded only for certain angles (Figure 13) and around 45° of angle, between 3 and 4 m on the virtual shot gather (Figure 26), Love waves can also be reconstructed that are not observed.

6.3.3 Conclusions

This preliminary analysis highlighted the need of wave propagation modeling in dam structure prior to any further analysis in order to understand what type of signals are recorded These questions are beyond the scope of this project and need to be answered before any classical analysis techniques can be applied on the inter-fibre correlations.

7 Improved evaluation of measurements from initial filling in 2020 (Phase 1)

7.1 IMPROVED EVALUATION METHODOLOGY

One of the main issues when measuring relative travel time change arises when the medium velocity changes by a large amount. Above a certain frequency, a given velocity change will induce a travel-time change larger than the dominant period of the seismic signal, which will induce a cycle-skipping effect(Figure 29).

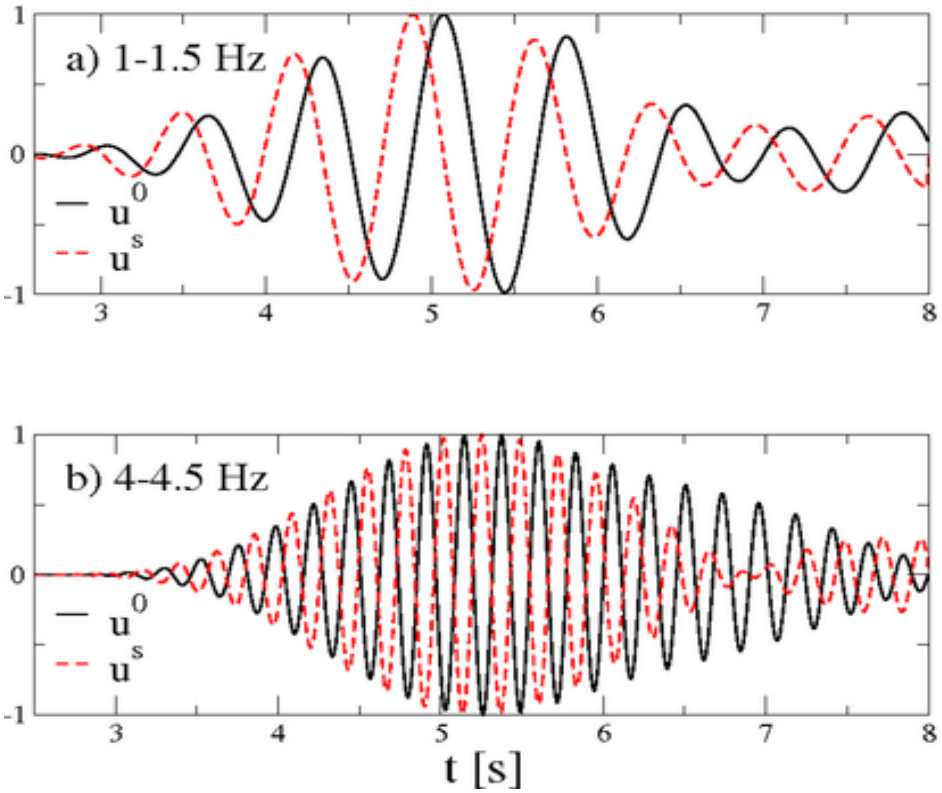

Figure 29 Illustration of the cycle-skipping effect as function of the frequency content of a seismogram. a) At low frequency, each phase of the reference correlation (black trace) is well identified and can be uniquely paired with the phases of the current correlation (red trace). At high-frequency, the phase association is no longer possible as there is an ambiguity in the phase correspondence. (Modified from Jiménez Tejero et al., (2015)).

This effect induces an ambiguity in the travel-time difference measurement relative to a fixed reference correlation. If a phase is wrongly identified it can create discontinuities in the relative velocity variation (dv/v) measurements, generating under- or overestimations of the velocity changes (Figure 30). After a certain level of velocity change, the reference correlation (which is taken as the average correlation during the first week of record) becomes too different and the cycle-skipping effect induces an apparent drop and unreliable measurements further in time.

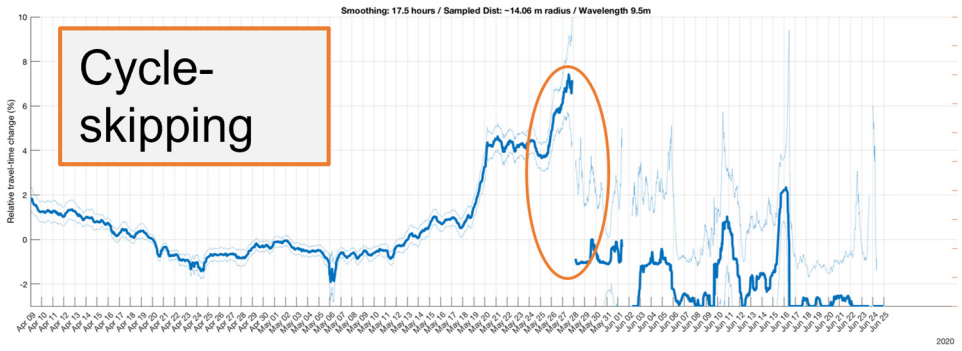

Figure 30 Example of the effect of cycle skipping on the velocity variation measurements.

To circumvent this problem, we chose an approach where no reference correlation is used in the dv/v measurements, but every individual correlation acts as a reference with respect to its neighboring (in calendar time) correlations. This way, the relative dv/v is measured between each possible pair of individual correlations then, by inversion, the time-series of dv/v can be reconstructed robustly. Indeed, instead of having 1 vs. N measurements, we now have N vs. N dv/v measurements. This redundancy is used to compensate for the potential measurement errors. We also give a stronger weight in the inversion to the dv/v measurements in close proximity (in calendar time) to the time we invert the dv/v for. Because the velocity changes are rather small and smoothed at the time-scale of a few hours, we expect fewer cycle-skipping problems when focusing on dv/v measurements between closely spaced correlations, further attenuating the issue of cycle-skipping.

7.2 RESULT

Figure 31 shows travel time variations (blue curve) together with water level measurements (red line), for the whole recording duration averaged for every channel pair. There is a significant travel-time decrease from the beginning of April until 23 April. The travel-time then stabilises until May 5, when it starts to slowly increase. Measurements of water level are available from this date. The travel-times displays consecutive step-like increases correlated with the water filling of the basin. Compared to previous results, we are now able to resolve the travel-time changes associated with each water-level elevation step. The amplitude of the travel-time steps is not fully correlated with the amplitude of the water-level steps: for the same water-level step, at low water-level, the travel-time change step is smaller than at high water level. This indicates an increased sensitivity to water level changes with increasing water-level.

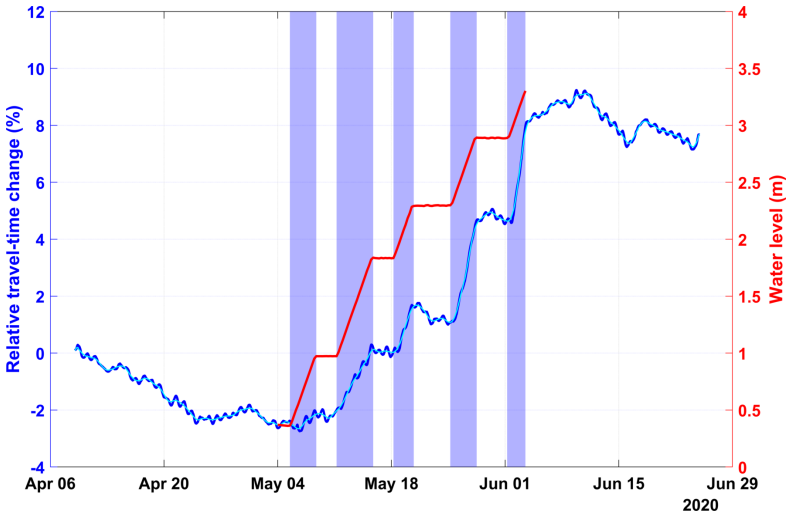

Figure 31 Average relative travel-time changes as a function of time for every channel pair (in blue). The water level changes are represented in red

To better quantify this observation, we model what would be the travel-time change induced by a water-level change given the specific sensitivity of Rayleigh waves with depth. Theoretical studies show that this sensitivity is decreasing exponentially with depth at a given frequency (Sens-Schonfelder and Wegler, 2006). This exponential decay depends on the mechanical properties of the medium. Finding the proper functional, we were able to reproduce the observed average travel-time changes based on the water-level curve as input data (Figure 32).

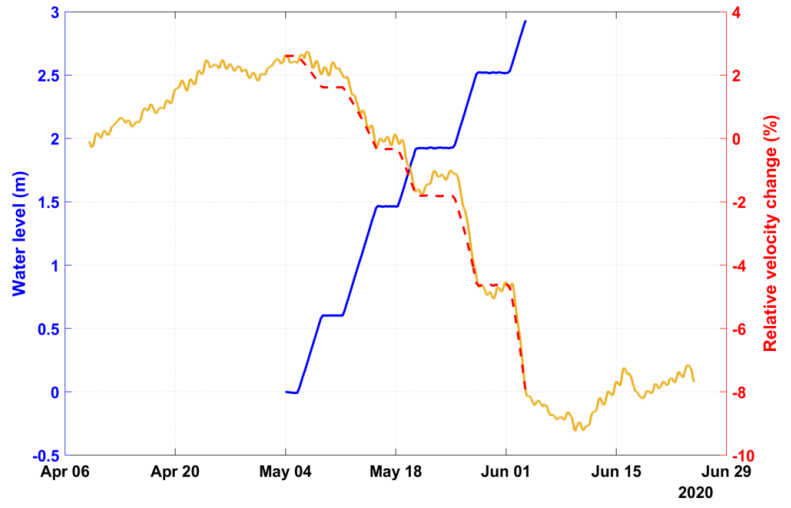

Figure 32 Measured averaged relative velocity changes as function of time (yellow curve) compared with the modelled relative velocity change (red dashed curve). The water-level is shown in blue.

We see that this simple model is able to reproduce to a high degree of fidelity the observed data, explaining why the dv/v curve is not perfectly linearly correlated with the water-level. Small discrepancies are still visible during the water-level plateaus where the model remains flat whereas the data exhibit an increase of velocity. This effect is probably due to a small drainage within the dam decreasing the level of the phreatic surface while the water-level in the reservoir remains constant. This effect is not taken into account in the modelling.

To obtain a spatio-temporal view of the velocity changes, we analysed the velocity variations (dv/v = -dt/t) on each channel pair separated by 2 m, with 1 m overlap. Figure 33 shows the velocity changes with time along the dam (colored background), together with the average velocity variation over all pairs (black curve). The contours at 0%, -2% and -4% of velocity changes are shown by the thin black lines. The grey, transparent shaded areas are the periods of water-level increase. Each individual spatially localised dv/v time-series is corrected so that their average level is 0% during the first 2 days of the experiment. This way, all velocity changes are relative to the start of the recording period and can all be compared with respect to the same reference.

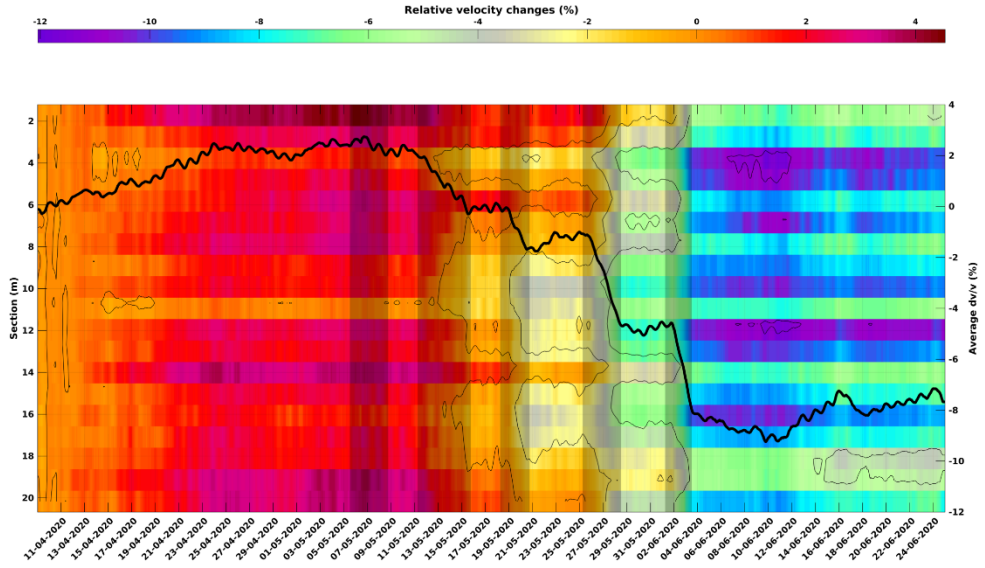

Figure 33 Relative velocity changes (in %) as function of time and dam chainage (colored background), together with the average velocity variation over all pairs (black curve). The contours at 0%, -2% and -4% of velocity changes are shown by the thin black lines. The grey, transparent shaded areas are the periods of water-level increase. Symbols represent the different clusters

We observe that although the localised dv/v time series exhibit the same pattern as the average curve, there are strong lateral variations. These lateral variations are particularly present during and after the water infill periods. Before the first infill period, most sections experience a slow increase of velocity, with lateral variations mostly confined between ±2% around the mean value. As examples of local behavior, around 6 and 14 m the velocity drop is delayed by one week or two, but quickly catches-up to the ~-4% level at section 6m. Inversely, Section 11m stays flat around 0% up to the second infill period and never reaches a level lower than -8% during the whole experiment. The edges of the dam also seem to have their own behaviour, with stronger increase of velocity before the dam infill and slightly smaller decrease during and after the infill periods.

7.3 INTERPRETATIONS

Our working hypothesis is that the observed lateral variations are in part due to the effects that the presence of the defects induces on the mechanical properties of the dam in response to the water-level variations. As seen in Figure 34, the lateral sensitivity of the dv/v measurements decreases exponentially away from the

considered channels, even if the sensitivity is non-zero even 10 m away from the sensors. Still, more than 50% of the sensitivity is confined in the close vicinity of the pair of channels, allowing us to interpret the observed dv/v at one position as the results of a local change in the medium.

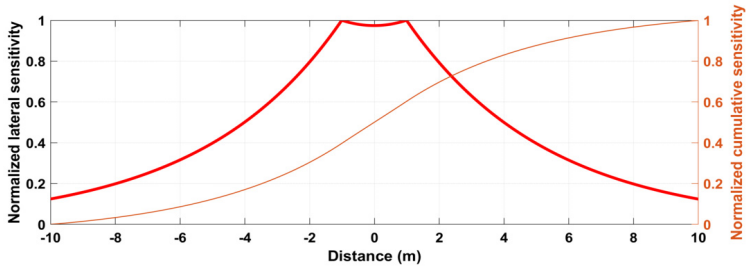

Figure 34 Lateral sensitivity of dv/v measurements. The positions of the two stations are at -1 m and 1 m. 50% of the sensitivity is confined at ±3m from the middle of the station pair.

To get a simpler view of the different behavior of the spatialized dv/v time series we regrouped them into 5 families depending on their degree of similarities between each other. We used a *kmean* clustering algorithm to perform this task. The results are shown in Figure 35. In the inset, each colored symbol corresponds to one cluster. Only the time-period encompassed by the black rectangle is used for the clustering analysis. In the main Figure 32, we display the average dv/v time series for each cluster, using the same color-coding scheme.

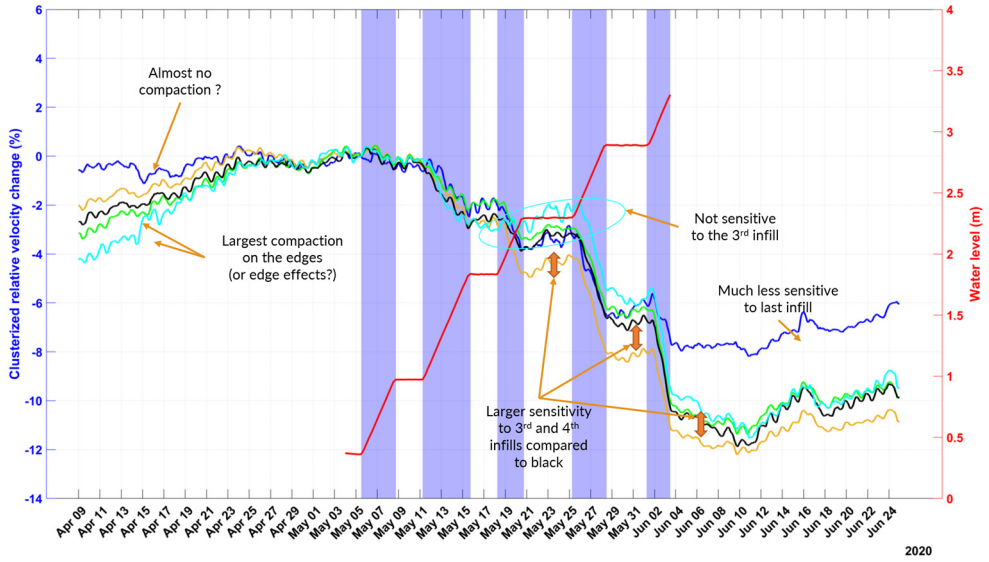

Figure 35 Velocity variations clustering and description/tentative interpretations of the main differences between each cluster.

We observe that the cyan cluster (made of only one dv/v time series at section 2 m) is similar to the green cluster except for the fact that its velocity increases faster at the beginning of the experiment and that it seems completely insensitive to the third water infill period. The blue cluster (also made of a single time series at section 11 m) has a peculiar behavior already noticed at the previous page. The black cluster has an intermediate behavior and is composed of 4 time-series (5 m, 7 m, 8 m, and 18 m). The yellow cluster corresponds to the parts of the dam experiencing the largest velocity drops during the third and fourth water infills.

8 Defect identification

8.1 SUMMARY OF MEASUREMENTS

DAS Measurements were done over two periods:

- Phase 1: from the 6th April to the 29th June 2020 during dam first filling
- Phase 2: from the 26th August to 11th November during dam emptying

In between these two phases, the water level was maintained constant. DAS data was analyzed using two different methods that we called "Imaging" and Monitoring. Imaging provided 2D sections of S-wave velocity according to depth. Monitoring provided the relative velocity compared to an average velocity over the entire dam section, every 30 min.

Only the CREST fiber data were analyzed, and all depths are calculated from the level of the crest cable. Preliminary analysis of inter-fiber correlations didn't provide results that are sufficiently complete to be interpreted

Based on simulations, the expected effect of the defects on seismic velocities within the defect and the surrounding medium were gathered in Table 3. Using this guideline, we attempted to identify the defects on results taken separately. All the defect identification are compared in a final step, and coinciding locations are taken as the most reliable defect identification. All the defects are smaller than the resolution inherent to the method. Simulations showed that defects also affect velocity of the surrounding material, making them detectable.

8.2 IMAGING

8.2.1 Phase 1

For the first phase, we obtained an image prior to filling using 5 days of DAS data (Figure 36).

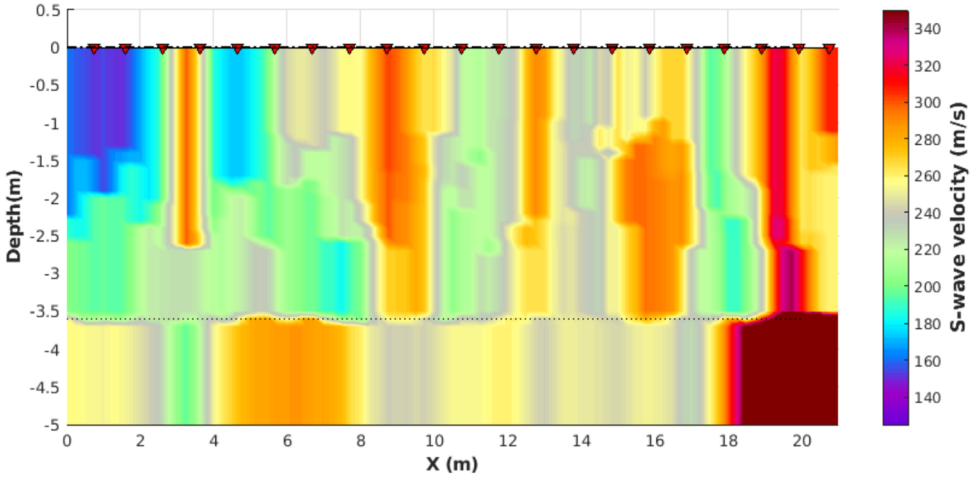

Figure 36: Vs Model obtained from the first phase of analysis. depths are calculated from the level of the crest cable. Depths are calculated from the level of the crest cable.

The defects made of concrete and wood are expected to have the highest velocities. These very high velocities are found between Sec 19 and 20 m. The other defects are also expected to have a higher velocity than the background velocity. We could delineate 7 high velocity zone from the single image (Figure 37).

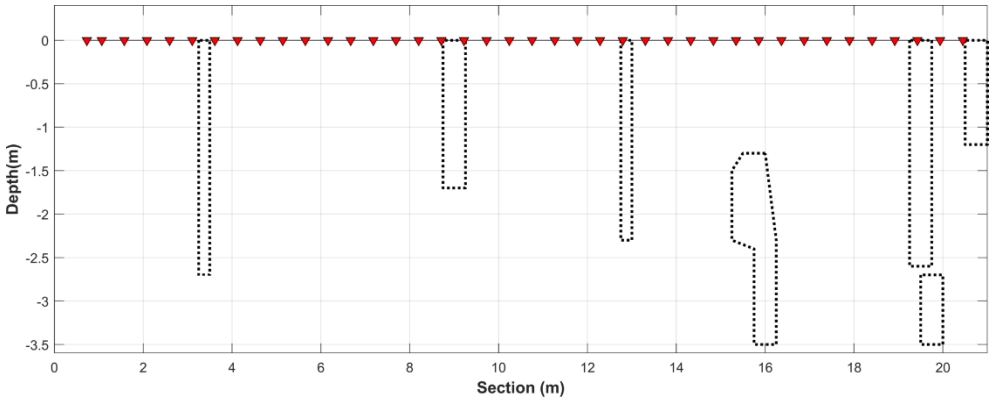

Figure 37: Defect identification on the Vs model obtained during Phase 1. Depths are calculated from the level of the crest cable.

8.2.2 Phase 2

For the second phase, we did a timelapse imaging of the dam during water draining (summarized in Figure 24). An increase of velocity is expected in the intact dam as in all the permeable defects, while the concrete and wood blocks should keep the same very high velocity. Timelapse imaging enables to highlight defects that are expected to respond quicker to draining than surrounding material (Table 3). These quick changes were triggered at different water level, helping to better determine the depth of the defect.

The same very high velocity zone is found between Sec 19 and 20 m. However, we observe an evolution of the velocity during filling or draining that was not expected. The findings are summarized in Figure 38.

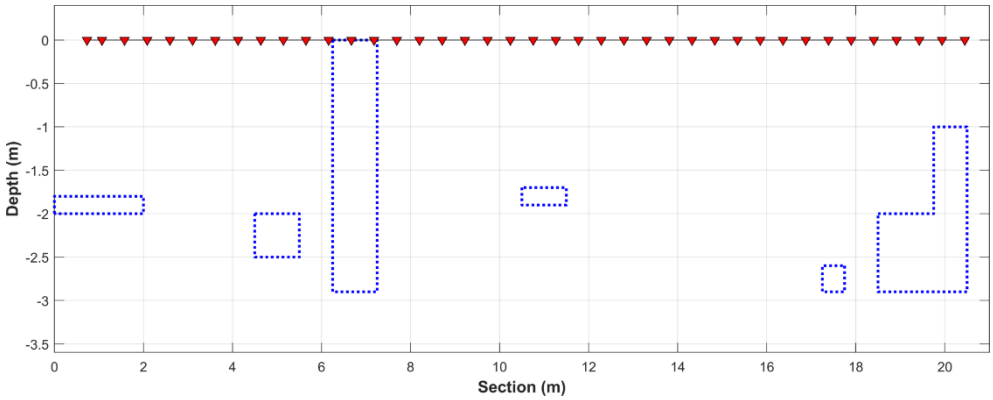

Figure 38 Figure Defect identification on the timelapse Vs models obtained during Phase 2 Monitoring. Depths are calculated from the level of the crest cable.

8.3 MONITORING

8.3.1 Phase 1

Based on the clustering analysis and observations, a first defect is identified at 11 m (blue cluster in Figure 35). At 3 m of water infill, this point stopped evolving. The light blue cluster also shows an opposite behavior to the expected ones (Table 3). We highlighted them because our expectations on velocity changes are not considering all the parameters that may affect velocity. The green and black clusters are very similar. They include all points that evolves the more slowly compared to others. In these two clusters are included the defects that should trigger no change but also the intact dam. The points of the yellow cluster are those showing the quicker and larger change. The yellow thus should gather the permeable defects. They were not affected by the first infill, meaning that they are most likely located at a higher level in the dam wall. As for timelapse imaging, the water level is used to better infer the height of the defects in the dam wall. The findings are summarized in Figure 39.

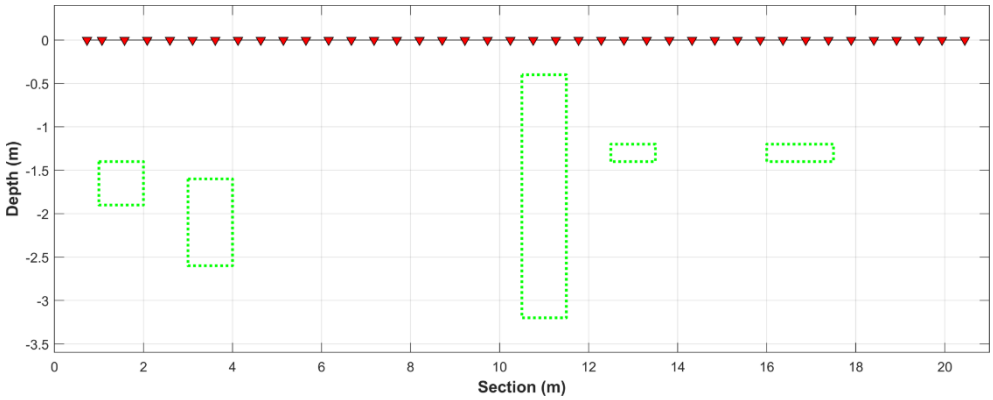

Figure 39: Defect identification on the monitoring results obtained during Phase 1. Depths are calculated from the level of the crest cable.

8.3.2 Phase 2

The Phase 2 results are a lot less spatially accurate because we could only use 5 m-spaced channels compared to the first phase where we used 2 m-spaced channels. The shadow areas to the section extremities are also wider. The clustering algorithm was also used for the defect identification. Three clusters were found, the blue circle being the intact dam, the yellow and green clusters being the defects (Figure 40). At 11 and 18 m, the trend of dv/v changes, we also note these behaviors as potential defects. The findings are summarized in Figure 41.

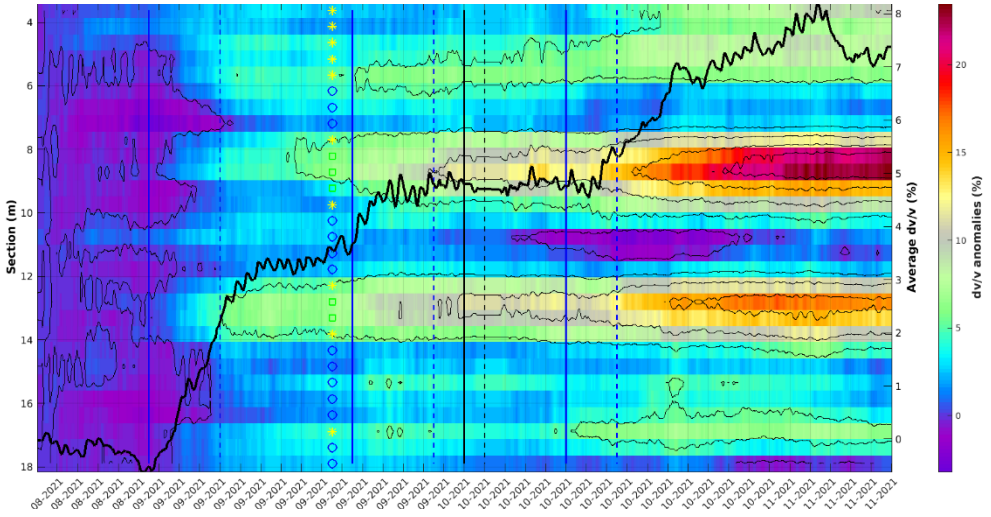

Figure 40: Clustering analysis of the monitoring results of phase 2.

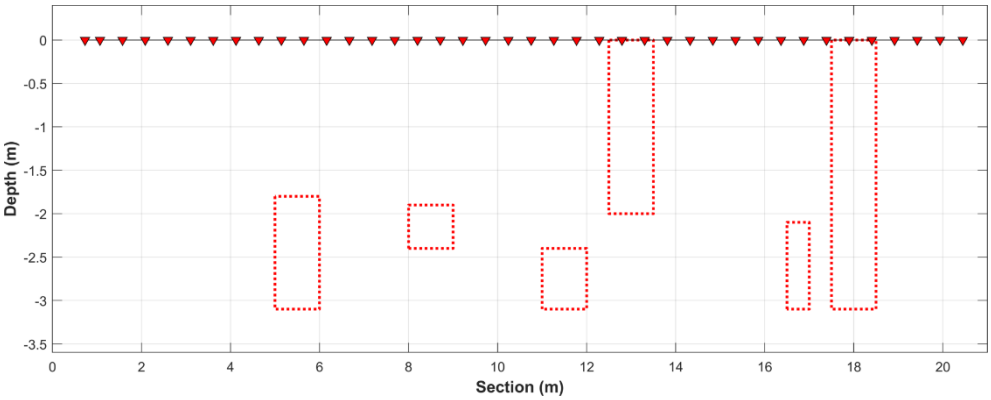

Figure 41: Defect identification on the monitoring results obtained during Phase 2. Depths are calculated from the level of the crest cable.

8.4 MERGE OF POTENTIAL DEFECT LOCATIONS

We gathered all the defect locations inferred from the different method and phase and gathered them in the same image (Figure 42). At the maximum, three different shapes overlap. The overlapping area is highlighted in red and correspond to the most reliable defect locations, around Sec 11 and 13 m. When two shapes overlap, they were highlighted in blue. At Sec 17-20 m, the defects correspond to very high velocity zones of the Vs models, interpreted as the wooden and concrete cubes. We expected that they can't be detected by monitoring. The comparison of defect identification shows that monitoring results are affected by these defects. This means that these defects, at least, induce a velocity change in the surrounding materials, but, if not only, in the defect as well.

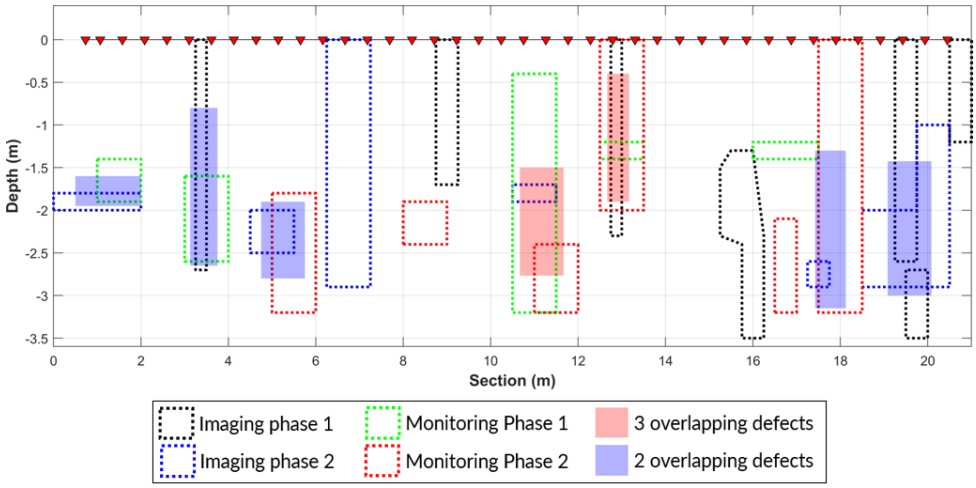

Figure 42: Defect identification summary

We highlighted a total of seven potential defect locations that were identified by at least two methods. The most probable ones are in the second half of the dam. The defects being too small to be imaged and monitored directly, this is mostly the effects in the surrounding material that were identified.

The results from Phase 2 seems to be the most reliable due to the improved monitoring accuracy compared to Phase 1, and the less transient effects at lowering the water level. Anomalies identified both in Imaging and Monitoring at Phase 2, would thus be the strongest sign of a defect.

At about Sec 11, 13, 17, and 19 m we see a good agreement between Imaging and Monitoring methods at Phase 2, but also sign in one of the methods used in Phase 1. At Sec 5 m we see agreement of both methods in Phase 2. These anomalies seem to be the most probable location of the defects.

We have already concluded that the anomalies at Sec 17 and 19 m might be the concrete and wooden cube, however with some changes or the core material/water leakage around. The horizontal damage crossing the core might be seen in Sec 5 or 11 m in the lower part of the dam. The vertical cylinder with coarse material may be the anomaly seen at Sec 13 m.

9 Conclusions and Recommendations

A second Phase of fibre-optic monitoring at the Test Dam with a DAS interrogator have been performed. Measurements of the ambient noise at Phase 2 were taken for two months when lowering the upstream water level, i.e. the opposite situation that occurred at Phase 1. We also used a more advanced DAS interrogator at Phase 2. This provided high-quality data suitable for improved ambient noise interferometry analysis.

Data evaluation have been performed based both using Imaging at some stages and Monitoring during the entire period. Further evaluation has also been carried out of the monitoring data from Phase 1.

The changes of the shear velocity have been estimated for different water levels and for the different defects. The impact from the defects maybe about a few m/s or about few %. The changes caused by water level changes will be larger.

The result from Imaging and Monitoring based on data collected in the crest cables shows that that the monitoring method enables to detect very small velocity changes, with a very good accuracy. The imaging method is less accurate both in term of time and velocity, but its advantage is the higher spatial information. Thus, the combination of both methods provides the location of the velocity changes. The first drainage period led to strong changes in the core of the dam, as imaged, while the second and third drainage period generated the strongest velocity changes outside of the sensitivity area of the wave used for imaging. We also found that the coda wave monitoring is sensitive to a larger bulk of the medium compared to the imaging using direct waves.

Preliminary analysis of inter-fiber correlations showed that we mainly detected reflections and only weak direct and coda waves. Imaging technique is using direct waves, and monitoring technique is using coda waves. No existing technique is using reflected surface waves. Because of the 1D directional sensitivity of DAS systems, correlations between different cables require careful consideration of the relationship with geometry of wave propagation in such a 3D structure as earthen dams. This preliminary analysis highlighted the need of wave propagation modeling in dam structure prior to any further analysis in order to understand what type of signals are recorded These questions are beyond the scope of this project and need to be answered before any classical analysis techniques can be applied on the inter-fibre correlations.

Compared to previous monitoring results from Phase 1, we are now able to resolve the travel-time changes associated with each water-level elevation step. The amplitude of the travel-time steps is not fully correlated with the amplitude of the water-level steps: for the same water-level step, at low water-level, the travel-time change step is smaller than at high water level. This indicates an increased sensitivity to water level changes with increasing water-level.

The results from Phase 2 seems to be the most reliable due to the improved monitoring accuracy compared to Phase 1, and the less transient effects at lowering the water level. Anomalies identified both in Imaging and Monitoring at Phase 2,

would thus be the strongest sign of a defect. We therefore make the following interpretation regarding the location and nature of the defects:

At about Sec 11, 13, 17, and 19 m we see a good agreement between Imaging and Monitoring methods at Phase 2, but also sign in one of the methods used in Phase 1. At Sec 5 m we see agreement of both methods in Phase 2. These anomalies seem to be the most probable location of the defects.

We have already concluded that the anomalies at Sec 17 and 19 m might be the concrete and wooden cube, however with some changes or the core material/water leakage around. The horizontal damage crossing the core might be seen in Sec 5 or 11 m in the lower part of the dam. The vertical cylinder with coarse material may be the anomaly seen at Sec 13 m.

From the survey results we are able to derive some guidance/recommendations for imaging and monitoring using ANI and DAS (Table 5). The progress that we see from the measurement and evaluation in Phase 2 is promising, and further improvements in techniques and technology are expected in the future.

Table 5: Limitations and drawbacks of each ANI method

	Imaging (Vs)	Monitoring (dv/v)
Spatial resolution	Low, because we use surface waves. Depends on the velocity of the medium and sensor spacing.	Low, sensitive to a large bulk of medium because we use coda waves. Depends on the sensor spacing that can be used. Here the spatial resolution was better during phase 1 because 2 m spacing were used compared to phase 2 with 5 m spacing.
Accuracy	About 10% of absolute velocity with 5 days of recordings. Can be improved by longer recording duration.	Depends on the case. Here, and today, we estimate an accuracy below 1% using DAS.
Minimum recording duration	Depends on noise level, and sensor sensitivity, here we used five days.	Depends on noise source stability, but in general at least one month or at least few days before a change of reservoir level.
Continuous recordings	Over 5 days, ideally when reservoir water level is constant.	To detect a dam defect appearing, monitoring needs to be done. Daily measurements of 30 min are recommended.
Noise sources	Needs to be in line with the optic fiber. Frequency content not controlled.	Needs to be stable through recording period (no frequency content changes).

The results and the experience gained in this project are promising and measurements on large dams can be performed using the methods developed, both for investigation purpose (short-time measurements) and for continuous monitoring. Further research is recommended to continue the method development, especially for better understanding of the cause of seismic velocity changes in the dam.

10 References

Becker, M. W., & Coleman, T. I. (2019). Distributed Acoustic Sensing of Strain at Earth Tide Frequencies. *Sensors*, *19*(9), 1975. doi: 10.3390/s19091975.

Curtis, A., Gerstoft, P., Sato, H., Snieder, R., Wapenaar, K., (2006). Seismic interferometry turning noise into signal. *Leading Edge 25*, 1082–1092.

de Ridder, S. A. L., B. L. Biondi, and R. G. Clapp (2014). Time-lapse seismic noise correlation tomography at Valhall, *Geophys. Res. Lett., 41*, 6116–6122, doi:10.1002/2014GL061156.

ICOLD (2015), Internal erosion of existing dams, levees and dikes, and their foundations, Bulletin 164 Volume 1: Internal erosion processes and engineering assessment, ICOLD Bulletin 164, 156p.

Jousset, P., Reinsch, T., Ryberg, T., Blanck, H., Clarke, A., Aghayev, R., Krawczyk, C. M. (2018). Dynamic strain determination using fibre-optic cables allows imaging of seismological and structural features. *Nature Communications*, *9*(1). doi: 10.1038/s41467-018-04860-y.

Johansson, S. (1997) Seepage monitoring in embankment dams. Doctoral Thesis, TRITA-AMI PHD 1014, ISBN 91-7170-792-1, Royal Institute of Technology, Stockholm.

Johansson, S., & Nilsson, Å. (2005). Internal Erosion Detection at the Røsvatn Test Site - Experiences from blind test using Resistivity, Self-Potential, Temperature, and Visual inspection. Part A – Assessment report. Elforsk rapport 05:42, Stockholm.

Johansson S., Stork A., David A., Mondanos M., and Nygren C. (2020). Fibre-optic Distributed Acoustic Sensing for detection of seepage and internal erosion, Energiforsk, Report 2020:682, ISBN 978-91-7673-682-1.

Lindsey N. J., Martin, E. R., Dreger, D. S., Freifeld, B., Cole, S., James, S. R., Biondi, B.L. & Ajo-Franklin, J. B. (2017). Fibre-optic network observations of earthquake wavefields. *Geophysical Research Letters, 44*, 11, 792–11,799. doi:10.1002/2017GL075722.

Mordret, A., et al. (2022). Detecting earthen dam defects using seismic interferometry monitoring on Distributed Acoustic Sensing data, *EGU Annual Meeting Proceedings.*

Nikles, M. (2009). Long-distance fibre optic sensing solutions for pipeline leakage, intrusion, and ground movement detection. *Fibre Optic Sensors and Applications VI.* doi: 10.1117/12.818021.

Parker, T., Shatalin, S., & Farhadiroushan, M. (2014). Distributed Acoustic Sensing – a new tool for seismic applications. *First Break*, *32*(2010). doi: 10.3997/1365-2397.2013034.

Tregourès, N.P. and van Tiggelen, B.A. (2002). Generalized diffusion equation for multiply scattered elastic waves. Waves Rand. Med., 12(21–38).

Zhan, Z., (2020). Distributed acoustic sensing turns fibre-optic cables into sensitive seismic antennas, *Seismological Research Letters*, **91**(1), 1–15.

Distributed Acoustic Sensing for Detection of Defects in the Test Dam at Älvkarleby – Phase 2

Optiska fibrer finns i flertalet fyllningsdammar i Sverige och är numera så gott som standard vid ombyggnad och nybyggnad. Fibrerna användas vanligen för detektion av vattenströmning och rörelser, men kan i många fall även användas för distribuerad akustisk mätning (Distributed Acoustic Sensing). Under de senaste åren har tekniken utvecklats markant, vilket medfört ytterligare möjligheter att studera hastighetsförändringar som uppkommit vid läckage/inre erosion i fyllningsdammar. Resultaten och erfarenheterna från detta projekt är lovande och mätningar kan göras både för undersökning (kortvariga mätningar) och för kontinuerlig övervakning. För bäst resultat rekommenderas att mätning görs under längre tid, gärna vid olika vattenstånd.

Energiforsk is the Swedish Energy Research Centre – an industrially owned body dedicated to meeting the common energy challenges faced by industries, authorities and society. Our vision is to be hub of Swedish energy research and our mission is to make the world of energy smarter.
www.energiforsk.se

Energiforsk